LncRNA *Dnmt3aos* regulates *Dnmt3a* expression leading to aberrant DNA methylation in macrophage polarization

Xueqin Li[1,2,+], Yingying Zhang[2,3,+], Mengying Zhang[1,2], Xiang Kong[1,2], Hui Yang[1,2], Min Zhong[1,2], Weiya Pei[1], Yang Xu[1,2], Xiaolong Zhu[1,2], Tianbing Chen[1,2], Jingjing Ye[1], and Kun Lv[1,2,*]

[1] Central Laboratory of Yijishan Hospital, Wannan Medical College, Wuhu, 241001, PR China

[2] Non-coding RNA Research Center of Wannan Medical College, Wuhu, 241001, PR China

[3] Laboratory Medicine of Yijishan Hospital, Wannan Medical College, Wuhu, 241001, PR China

*Corresponding To: Dr. Kun Lv, Central Laboratory of Yijishan Hospital, Wannan Medical College, 2 Western Zheshan Road, Wuhu 241001, People's Republic of China

E-mail: lvkun315@126.com

Tel: 86-553-5739912

[+]These authors contributed equally to this work.

Abstract

Long non-coding RNAs (lncRNAs) play key roles in various biological processes. However, the roles of lncRNAs in macrophage polarization remain largely unexplored. In this study, thousands of lncRNAs were identified that are differentially expressed in distinct polarized bone marrow-derived macrophages (BMDMs). Among them, *Dnmt3aos* (DNA methyltransferase 3A, opposite strand), as a known lncRNA, locates on the antisense strand of *Dnmt3a*. Functional experiments further confirmed that *Dnmt3aos* were highly expressed in M(IL-4) macrophages and participated in the regulation of *Dnmt3a* expression, and played a key role in macrophage polarization. The DNA methylation profiles between the *Dnmt3aos* knockdown group and the control group in M(IL-4) macrophages were determined by MeDIP-seq technique for the first time, and the *Dnmt3aos-Dnmt3a* axis-mediated DNA methylation modification-regulated macrophage polarization related gene *IFN-γ* was identified. Our study will help to enrich our knowledge of the mechanism of macrophage polarization and will provide new insights for immunotherapy in macrophage-associated diseases.

Keywords: LncRNA, DNA methylation, Dnmt3a, macrophage polarization

Abbreviations:

LncRNA, Long non-coding RNA; Dnmt3aos, DNA methyltransferase 3A opposite strand; Dnmt3a, DNA methyltransferase 3a; BMDM, bone marrow-derived macrophages; MeDIP-seq, methylated DNA immunoprecipitation sequencing; LPS, lipopolysaccharides; IFN-γ, interferon-gamma; GM-CSF, granulocyte-macrophage colony stimulating factor; IL-4, interleukin-4; IL-12, interleukin-12; IL-13, interleukin-13; TNF-α, tumor necrosis factor alpha; NO, nitric oxide; CD80, cluster of differentiation 80; CD68, cluster of differentiation 68; M-CSF, macrophage colony stimulating factors; TGF-β, transforming growth factor beta-1; Arg-1, Arginase 1; YM1, chitinase 3-like 3; Fizz1, Resistin-like-α; DMR, differentially methylated region; UTR, untranslated region; CDS, coding sequence; TTR, transcriptional termination region; GO, gene ontology; DEG, differentially expressed gene; 5-Aza-CdR, 5-Aza-2′-deoxycytidine; BSP, bisulfite sequencing PCR; ncRNA, non-coding RNA.

Introduction

Macrophages, as an essential component of the innate immune system, are widely distributed throughout the organs and tissues and possess high heterogeneity and plasticity. Macrophages can be broadly classified into two extremely polarized phenotypes, “Classical” and “Alternative,” which exhibit different functions under the influence of distinct microenvironmental stimuli. Classically activated macrophages have long been known to be induced by lipopolysaccharides (LPS) and interferon-gamma (IFN-γ) or granulocyte-macrophage colony stimulating factor (GM-CSF), and are characterized by high levels of pro-inflammatory cytokines such as interleukin-12 (IL-12) and tumor necrosis factor alpha (TNF-α) and oxidative metabolites such as nitric oxide (NO). M(LPS+IFN-γ) macrophages generally promote Th1-type immune responses, with upregulation of MHC II and the costimulatory molecules CD80 and CD86, which are essential for antigen presentation and which strengthen phagocytosis and killing of pathogenic microorganisms or tumor cells [1,2]. In contrast, the alternative M(IL-4) macrophages are induced by Th2 cytokines (such as IL-4 and IL-13) or macrophage colony stimulating factors (M-CSF), with high secretion levels of anti-inflammatory cytokines such as IL-10 and transforming growth factor beta-1 (TGF-β), and high expression of Arginase 1 (Arg-1), chitinase 3-like 3 (Chi3l3 or YM1), and Resistin-like-α (Retnl α or Fizz1). These macrophages participate in tissue repair, angiogenesis, tumor progression, and defense against parasite infection [1,3,4]. Therefore, macrophage polarization is a vital component in the progression of many

89 diseases, including infection [5], tumors [2,6], obesity, and insulin resistance [7,8].
90 Further study of the molecular mechanisms regulating macrophage polarization will
91 enhance our understanding of the pathogenesis and development of
92 macrophage-centered diseases and provide a basis for the diagnosis and treatment of
93 such diseases. However, the regulatory mechanism of the macrophage activation
94 conditioning response remains to be further elucidated.

95 LncRNAs are RNA molecules > 200 nucleotides long. They are therefore
96 structurally similar to mRNA, but they do not encode proteins. The lncRNAs are
97 emerging as important regulators of gene transcriptional regulation, chromatin
98 remodeling, nuclear transportation, and other biological processes [9]. They play
99 pivotal roles in various human diseases. Recent studies have confirmed that lncRNAs
100 correlate with macrophage differentiation and activation [10-14]. Epigenetic
101 regulation, including DNA methylation, is critical in cell differentiation and
102 development. *De novo* DNA methylation is catalyzed by DNA methyltransferase
103 (DNMT) 3a and 3b. DNA methylation of cytosines at CpG dinucleotides is the most
104 common epigenetic modification, and CpGs are often enriched in the promoter region
105 of genes [15]. Promoters of hypo-methylated genes are typically associated with
106 transcriptionally active genes [16], whereas DNA hyper-methylation can result in
107 gene silencing [17,18]. However, there are few reports on the role of epigenetic
108 modification in macrophage polarization so far. Recently, histone methylation and
109 Dnmt3b mediated DNA methylation have been implicated in the regulation of
110 macrophage polarization [15,19-21]. However, at present, no studies have been

reported on the lncRNAs regulating Dnmt3a expression-mediated aberrant methylation of DNA in macrophage polarization.

In the current study, we utilized microarray and bioinformatics methods to acquire differentially expressed lncRNAs profiles existing in M(LPS+IFN-γ) and M(IL-4) macrophages, and we identify novel lncRNAs, which are functional in macrophage polarization. Among the thousands of lncRNAs that are actively regulated in macrophage polarization, we further determined that lncRNA *Dnmt3aos*, a known lncRNA locates on the *Dnmt3a* antisense strand, is a key regulator of *Dnmt3a* expression and also regulates macrophage polarization. We also used a methylated DNA immunoprecipitation sequencing (MeDIP-seq) method combined with mRNA expression profile analysis to screen the *Dnmt3aos-Dnmt3a* axis-mediated DNA methylation-modified macrophage polarization related genes, and we explored the roles of related genes in macrophage polarization. Our study will help to enrich our understanding of the mechanism of macrophage polarization and will provide new approaches to immunotherapy in macrophage-centered diseases.

Results

Identification of *ex vivo* polarized M(LPS+IFN-γ) and M(IL-4) macrophage LncRNAs, including *Dnmt3aos*

To use a systematic approach to identifying alterations in the lncRNA expression profile during macrophage polarization, we examined the lncRNA and mRNA expression profiles in polarized BMDMs through microarray analysis. First, we

prepared the M(LPS+IFN-γ) and M(IL-4) macrophages *in vitro*. BMDMs were isolated from BALB/c mice and stimulated with LPS and IFN-γ to obtain M(LPS+IFN-γ) or with IL-4 to obtain M(IL-4). The polarization conditions used in this study resulted in distinct macrophage phenotypes as confirmed in our previous study [22-24].

For the microarray analysis, authoritative data sources containing more than 33,231 lncRNAs were used. To identify the most significant candidates, lncRNAs with at least two-fold differentially expressed changes and with FDR adjusted *P* values < 0.05 were selected (Fig 1a and 1b and S1 Data). Under these criteria, 627 lncRNAs were up-regulated, and 624 lncRNAs were down-regulated in the M(LPS+IFN-γ) group compared with the M(IL-4) group. In addition, 696 mRNAs were up-regulated and 557 mRNAs were down-regulated in the M(LPS+IFN-γ) group compared with the M(IL-4) group (Tab 1 and S1 Data). The mRNA expression profiles were reported in our previous publication [22].

To confirm the microarray results, four differentially expressed lncRNAs were selected for further confirmation using RT-qPCR (Fig 1c). Among the four selected lncRNAs, *AK048798* and *AW112010* were upregulated in M(LPS+IFN-γ) macrophages compared to M(IL-4) macrophages, while *4933417E11Rik* and *Dnmt3aos* were downregulated in M(LPS+IFN-γ) macrophages compared to M(IL-4) macrophages (Fig 1c). The results were generally consistent with the microarray data.

Since many lncRNAs have been shown to regulate neighboring genes either positively or negatively [25-27] as their target genes, the genomic locations of these

lncRNAs were further characterized. We decided to focus on lncRNA *Dnmt3aos* since it is a known lncRNA, locates on the *Dnmt3a* gene antisense strand on mouse chromosome 12 (Fig 1d).

Characterization of the *Dnmt3aos* expression pattern

To further determine the cellular localization of the *Dnmt3aos* transcript, the nuclear and cytosolic RNAs were isolated from BMDMs, and the expressions of *Dnmt3aos* transcripts in both subcellular locations were measured. RT-qPCR data show that *Dnmt3aos* transcripts are highly expressed in the nucleus compared with the cytosol (Fig 1e). As controls, *GAPDH* mRNA is specifically located in the cytosol, whereas *U6* RNA is primarily located in the nucleus (Fig 1e). RNA fluorescence in situ hybridization (RNA FISH) indicates that *Dnmt3aos* is highly expressed in the nucleus (Fig 1f).

We next examined the expression profile of *Dnmt3aos* in multiple mouse tissues. *Dnmt3aos* was expressed in many mouse tissues (S1 Fig), including lung, brain, spleen, pancreas, liver, heart, kidney, and fat.

Elevated expression of *Dnmt3aos* in M(IL-4) polarized macrophages contributes to macrophage polarization

Dnmt3aos had increased expression in M(IL-4) macrophages (Fig 2a). Therefore, we further characterized its role in macrophage activation. We assessed the level of *Dnmt3aos* in macrophages after the dynamic process of macrophage re-polarization.

177 Macrophages with the M(LPS+IFN-γ) or M(IL-4) phenotypes were re-polarized to the
178 M(IL-4) or M(LPS+IFN-γ) phenotype by treatment with LPS/IFN-γ or IL-4,
179 respectively. The marker gene (we used iNOS as the marker for M(LPS+IFN-γ)
180 macrophages and Arg1 as the marker for M(IL-4) macrophages [22]) assays clearly
181 showed that M(LPS+IFN-γ) macrophages could be re-polarized to M(IL-4)
182 macrophages by IL-4 (S2a Fig), and M(IL-4) macrophages could be re-polarized to
183 M(LPS+IFN-γ) macrophages by LPS/IFN-γ (S2b Fig). Interestingly, the *Dnmt3aos*
184 levels in macrophages were strikingly elevated during M(LPS+IFN-γ)-to-M(IL-4)
185 re-polarization of macrophages (Fig 2b), but *Dnmt3aos* levels decreased following
186 M(IL-4)-to-M(LPS+IFN-γ) re-polarization of macrophages (Fig 2c). These results
187 suggest that *Dnmt3aos* may play a critical role in promoting macrophage polarization
188 to the M(IL-4) phenotype.
189

190 **_Dnmt3aos_ regulates _Dnmt3a_ RNA and protein in BMDMs**

191 To test the correlation between *Dnmt3aos* levels and macrophage polarization, the
192 gene was examined after primary BMDMs were treated with LPS/IFN-γ or IL-4
193 stimulation. The *Dnmt3aos* gene was down-regulated with the polarization of
194 M(LPS+IFN-γ) macrophages, but up-regulated with the M(IL-4) polarization (Fig 3a)
195 when compared to the primary BMDMs. Meanwhile, the expression level followed a
196 time course dependent on the LPS/IFN-γ or IL-4 stimulation (Fig 3a), and correlated
197 to the M(LPS+IFN-γ) and M(IL-4) phenotype, marked by iNOS and Arg1 gene
198 expression, respectively (S3 Fig). Notably, this expression pattern was almost

199 identical to that of Dnmt3a mRNA (Fig 3b). This observation suggests that *Dnmt3aos*
200 and *Dnmt3a* expression may be regulated concordantly, as was recently shown for
201 other sense-antisense pairs [28-31].

202 We next investigated whether the *Dnmt3aos* transcript regulates expression of
203 *Dnmt3a* mRNA. RT-qPCR results showed that transfection of primary BMDM cells
204 with Dnmt3aos smart silencer (si-Dnmt3aos) resulted in a statistically significant
205 knockdown of not only the targeted *Dnmt3aos* transcript, but also of *Dnmt3a* mRNA
206 and protein levels (Fig 3c and 3e). In contrast, the expression of the si-Dnmt3a in
207 primary BMDMs resulted in a significant reduction of the targeted *Dnmt3a* mRNA
208 and protein levels (Fig 3d and S4 Fig), but did not affect the expression of *Dnmt3aos*
209 transcripts (Fig 3d). This suggests that *Dnmt3aos* may regulate the expression of
210 *Dnmt3a* at both the mRNA and the protein levels in primary BMDMs. These
211 observations further confirm the regulation of *Dnmt3a* expression by *Dnmt3aos*, not
212 only at the mRNA but also at the protein level.

213

214 **Knockdown of *Dnmt3aos* expression promotes M(LPS+IFN-γ) macrophage**
215 **polarization and decreases M(IL-4) macrophage polarization**

216 The expression profile of *Dnmt3aos* prompted us to investigate its function during
217 macrophage polarization. To determine if *Dnmt3aos* participates in macrophage
218 polarization, we transfected primary BMDM macrophages with Dnmt3aos smart
219 silencer. Interestingly, when primary BMDM macrophages were transfected with
220 Dnmt3aos smart silencer and then treated with LPS/IFN-γ or IL-4, the M(LPS+IFN-γ)

221 phenotype was increased. Specifically, the M(LPS+IFN-γ) macrophage phenotype
222 markers iNOS, TNF-α, and IL-12 were all up-regulated, but the M(IL-4) macrophage
223 markers Arg1, YM1, and FIZZ1 were strikingly down-regulated (Fig 4). These results
224 suggested that *Dnmt3aos* may play a critical role in promoting macrophage
225 polarization.
226
227 **The *Dnmt3aos-Dnmt3a* axis regulates macrophage polarization-related gene**
228 **expression through modification of DNA methylation**
229 The establishment and maintenance of *de novo* DNA methyltransferase 3A (Dnmt3a)
230 mediated methylation patterns resulting in modulation of gene expression is one of the
231 key steps in epigenetic regulation during cell differentiation and biological processes
232 [32-35]. Since the *Dnmt3aos* and *Dnmt3a* genes were differentially expressed in
233 macrophage polarization and were highly expressed in M(IL-4) macrophages (Fig 3a
234 and 3b), and based on the results that *Dnmt3aos* regulates *Dnmt3a* gene expression,
235 we carried out methylated DNA immunoprecipitation sequencing (MeDIP-seq) to
236 evaluate the possibility of association between DNA methylation variability and
237 macrophage polarization to identify differentially methylated regions (DMRs) related
238 to macrophage polarization. Indeed, unique DNA methylation features were identified
239 in negative control non-targeting siRNA- (si-NC-) and si-Dnmt3aos-transfected
240 M(IL-4) macrophages. We looked at methylation changes in four regions defined by
241 the distance from the CpG islands [36], namely, the CpG island, Shore, Shelf, and
242 Open Sea regions, the latter three being, respectively, 2 kb, 2-4 kb, and more than 4

kb from the CpG island. Most CG islands of the si-NC group and si-Dnmt3aos group both were detected in the Open Sea regions (Fig 5a). Next, we scrutinized the distribution of DMRs in the context of gene structure. Seven relevant regions were defined: promoter, five-prime untranslated region (UTR), coding sequence (CDS), three-prime UTR, intron, the transcriptional termination region (TTR), and the intergenic region. However, the DMRs were distributed differentially in the seven regions, and had no significant changes between the si-NC group and si-Dnmt3aos group. As shown in Fig 5b, DMRs were concentrated mainly in introns and in the intergenic region. Heat maps of DMRs methylation levels for the two biological replicates of the si-NC group and si-Dnmt3aos group are shown in Fig 5c. In total, 5,143 DMRs were selected based on the criterion of fold change (FC) > 1.5 and corrected *P* value (FDR) < 0.05 (S2 Data). The chromosomal locations of the DMRs are shown in Fig 5d. The red represents high methylation and the blue represents low methylation. The height represents logFC. Circos plots of global genomic methylation level across each chromosome with comparisons between the si-NC group and si-Dnmt3aos group are shown in Fig 5e. On the whole, the chromosomal locations between the si-NC and si-Dnmt3aos-transfected M(IL-4) macrophages were almost identical.

To generate insights into the potential biological functions of DMRs, functional enrichment analysis was performed using GO and KEGG pathway terms. Based on DMR-related genes, we provided a GO functional classification annotation for DMR-related genes. All differently expressed genes were mapped to each term of the

GO database (http://www.geneontology.org/) and the KEGG pathway database (https://www.kegg.jp/kegg/pathway.html), the gene numbers of the GO and KEGG terms were calculated. A hypergeometric test was used to determine significantly enriched GO and KEGG terms of the DMR-related genes compared to the genome background, and the corrected-*P* value ≤ 0.05 was used as a threshold. GO and KEGG terms fulfilling this condition were defined as significantly enriched GO and KEGG terms of DMR-related genes. Through this analysis, we were able to recognize the top 30 biological functions (Fig 6a and S3 Data) and top 30 pathways in which DMR-related genes participated (Fig 6b and S4 Data).

Our previous investigations of gene expression in macrophage polarization have shown that 1,253 unique genes are significantly differentially expressed genes (DEGs) [22]. Since we have previously confirmed that *Dnmt3aos* plays a critical role in macrophage polarization, knockdown of Dnmt3aos expression promotes the M(LPS+IFN-γ) macrophage phenotype and decreases the M(IL-4) macrophage phenotype (Fig 4). In order to explore the relationship between DNA methylation and gene expression in macrophage polarization, we combined the DNA methylation profiles from the si-NC and si-Dnmt3aos-transfected M(IL-4) macrophages and gene expression profiles (Data are presented in reference 22) to identify the DMR-related genes. As expected, hypomethylated DMRs were associated with increased gene expression (exhibited as blue dots in Fig 6c), and hypermethylated DMRs were associated with decreased gene expression (exhibited as green dots in Fig 6c). Others in which methylation changes were not associated with expected gene expression

differences are exhibited as pink and purple dots in Fig 6c and are listed in S5 Data. It is known that the high level of DNA methylation in promoter region inhibits the expression of its genes. Therefore, we choose DMR-related genes which are negatively correlated with the level of DNA methylation in promoter region and its expression level of mRNA for follow-up study. Heat maps were used to show the list of DMR-related genes distributed in promoter regions (Fig 6d). Among these genes, *Ifng*, *Icosl, Cd24a, Ncrna00085,* and *Tnf* genes were hypermethylated in the **s**i-NC group compared to the si-Dnmt3aos group. These genes were associated with increased expression in M(LPS+IFN-γ) macrophages compared to M(IL-4) macrophages. The *Pdia2* and *Entpd3* genes were hypomethylated in the **s**i-NC compared to the si-Dnmt3aos group. These genes were associated with decreased expression in M(LPS+IFN-γ) macrophages compared to M(IL-4) macrophages (see S6 Data).

Given the finding that the differential expression of *Dnmt3a* in polarized macrophages was dependent on *Dnmt3aos* and was responsible for the DNA methylation of DMR-related genes, we sought to determine whether the expression of DMR-related genes was also regulated by the *Dnmt3aos-Dnmt3a* axis. As expected, the results of this experiment showed that compared to the **s**i-NC group, knockdown of *Dnmt3aos* expression not only down-regulated the M(IL-4) macrophage phenotype related genes (Arg1, YM1, and FIZZ1), but also influenced the expression of the selected DMR-related genes like *IFN-γ, Icosl, Cd24a, TNF-α, Lrrk2*, *Lox, Pdia2 and Entpd3* (Fig 7a). Additionally, *IFN-γ, Icosl, Cd24a, TNF-α*, *Lrrk2,* and *Lox* were also

309 elevated in macrophages treated with specific siRNA targeting *Dnmt3a* for
310 knockdown in M(IL-4) (Fig 7b). The same results were observed in M(IL-4)
311 macrophages treated with the DNMT inhibitor 5-Aza-2′-deoxycytidine (5-Aza-CdR)
312 (Fig 7c).

313 To further validate the differential methylated CG sites in the DMR region from
314 the MeDIP-seq results (S7 Data), genomic DNA samples of the **s**i-NC and
315 si-Dnmt3aos-transfected M(IL-4) macrophages were treated with sodium bisulfate
316 and amplified by PCR with specific primers. After TA cloning, five positive clones
317 were selected for DNA sequencing. The methylation patterns of these genes are
318 displayed in white and black rectangles (Fig 7e), where the black and white rectangles
319 represent methylated CG and non-methylated CG loci, respectively. The bisulfite
320 sequencing PCR (BSP) sequencing results were analyzed and are summarized in Fig
321 7e and S5-8 Fig. The whole *IFN-γ* DMR region from the MeDIP-seq results contained
322 8 CG sites (Fig 7d), but the BSP sequencing successfully sequenced sites 1-2 and 6-8
323 in order. The white–black rectangle diagram shows that only the site 2 and site 7 CG
324 sites were hypermethylated in the si-NC group compared to the si-Dnmt3aos group
325 and were in accordance with the MeDIP-seq results (Fig 7e). Bisulfite pyrosequencing
326 was then performed to further validate the global DNA methylation percentages of the
327 single CG dinucleotide locus at the site 2 and site 7 CG sites in the *IFN-γ* DMR region,
328 which were differentially methylated according to the BSP results in the **s**i-NC and
329 si-Dnmt3aos-transfected M(IL-4) macrophages. The results showed that the site 2 CG
330 dinucleotide loci of *IFN-γ* CG sites had significant differences between the two group

331 macrophages, while the site 7 CG dinucleotide loci of *IFN-γ* CG sites were calculated
332 as having no difference (Fig 7f). The expression of *IFN-γ* was induced when its
333 promoter was demethylated, and this induction was achieved by Dnmt3a and
334 *Dnmt3aos* knockdown (Fig 7g). These results collectively suggested that
335 *Dnmt3aos-Dnmt3a* axis mediated DNA methylation modification was involved in
336 macrophage polarization.
337

338 **Discussion**

339 Macrophage polarization is associated with a variety of diseases, such as infection,
340 tumors, and obesity. Based on the polarization of macrophages into M1 and M2, two
341 extreme categories under different environmental stimuli, the functions of
342 macrophages are completely different and are even mutually inhibited. Appropriate
343 activation of macrophages helps to clear pathogens and tumors, while inappropriate
344 activation of macrophages may inhibit an organism's immune system, promoting
345 tumor occurrence or progression and chronic infection [37-40]. Macrophage
346 polarization is regulated by different mechanisms, including intracellular signaling
347 pathways, transcription factors, and epigenetic and post-translational modifications.
348 Recent studies have shown that non-coding RNA (ncRNA) also participates in the
349 regulation of macrophage polarization [23,41-43]. At the present time, lncRNA is a
350 hotspot in various research fields, and several reports have confirmed that lncRNA
351 plays vital roles in macrophage differentiation and activation [10-14]. Our study was
352 designed to identify novel and functional lncRNA molecules in two major patterns of

353 macrophage activation.

354 In the present study, we analyzed lncRNA expression profiles in polarized
355 BMDMs to uncover the potential role of lncRNAs in macrophage polarization via
356 high-throughput microarray techniques. Among the thousands of identified
357 differentially expressed lncRNAs, we found 627 that were up-regulated and 624 that
358 were down-regulated in M(LPS+IFN-γ) macrophages compared to M(IL-4)
359 macrophages. Following this, four lncRNAs (*AK048798*, *AW112010, 4933417E11Rik,*
360 and *Dnmt3aos*) were selected for further confirmation by RT-qPCR. *AK048798* was
361 selected because its potential target gene is Hif1α via trans-target prediction (data
362 were not shown). This gene encodes a protein that has been shown to modulate
363 macrophage polarization and to function in many diseases. *Dnmt3aos* was selected
364 because it is a known lncRNA with no reported functionality. It locates on the
365 antisense strand of Dnmt3a, which is an important component involved in epigenetic
366 regulation [44,45]. The other two lncRNAs were randomly selected. The data showed
367 that the RT-qPCR results were consistent with the microarray data.

368 Mechanistically, lncRNAs regulate gene expression via distinct processes that
369 promote or inhibit recruitment of epigenetic regulators to modulate chromatin
370 structure. Recent reports have shown that antisense lncRNA may function in
371 sense-antisense pairs [28-31]. Our results showed the same regulation pattern. We
372 saw that knockdown of *Dnmt3aos* expression altered the expression of *Dnmt3a* at
373 both the mRNA and the protein levels in primary BMDMs, but silencing *Dnmt3a* did
374 not alter the expression of *Dnmt3aos* (Fig 3). We also found that both the expression

375 levels of *Dnmt3aos* and *Dnmt3a* were correlated to macrophage polarization.
376 Meanwhile, we observed that *Dnmt3aos* was highly enriched in the nucleus, and
377 *Dnmt3a,* as one of the DNA methyltransferases, catalyzed *de novo* DNA methylation
378 in the nucleus. *Dnmt3a* plays an important role in cell development and tumorigenesis.
379 DNA methylation represents one of the major epigenetic modifications and plays key
380 roles in a variety of regulatory mechanisms of life processes [46-47]. The DNA
381 methyltransferase (DNMT) family contains DNMT1, DNMT3A, and DNMT3B.
382 DNA methylation in macrophage polarization is rarely reported [15] and
383 lncRNA-mediated epigenetic modifications have not been previously examined. In
384 our study, we determined that the DNA methylation levels in the two distinct kinds of
385 polarized macrophages were significantly different. Notably, the pattern of DNA
386 methylation also was found to be different in the two macrophage extremes.
387 MeDIP-seq results showed that there were significant differences in genome-wide
388 methylation levels between the **s**i-NC and si-Dnmt3aos-transfected M(IL-4)
389 macrophages. Combined analysis of DMR-related genes and mRNA expression
390 profiles (reported in the literature 22) revealed a significant correlation between
391 differential DMR-related genes and differential mRNA (Fig 5 and Fig 6). Our new
392 results demonstrate that the *Dnmt3aos-Dnmt3a* interaction could be a key mechanism
393 in macrophage polarization.

394 In fact, an altered genomic DNA methylation pattern characterized by regionally
395 modified patterns of hypo- and hypermethylation exists in the **s**i-NC and
396 si-Dnmt3aos-transfected M(IL-4) macrophages. Notably, there was no major change

in the methylation pattern at CpG islands, and the abnormal hypo- and hypermethylation status existed mostly in regions where CpG sites were sparse. Theoretically, reducing DNA methylation at gene promoters is associated with gene activation [48]. Our data also showed that inhibition of *Dnmt3aos* or *Dnmt3a* expression significantly increased the expression of the DMR enriched macrophage polarization related genes *IFN-γ, Cd24a, Icosl, Lox, TNF-α,* and *Lrrk2*. Then we confirmed the DNA methylation level by using BSP sequencing and bisulfite pyrosequencing. The results showed that among the randomly selected five TA clones used in the BSP DNA sequencing of *Lox* gene, the DNA methylation levels were hypomethylated in the si-NC group compared to the si-Dnmt3aos group (S5a and S5b Fig), and for *Icosl* gene, there was no difference between two groups (S5c and S5d Fig). The other four genes (*IFN-γ, Cd24a, TNF-α,* and *Lrrk2*) all contain the CG sites that were hypermethylated in the si-NC group compared to the si-Dnmt3aos group. We believe that BSP and pyrosequencing can also detect DNA hypomethylation and mixed methylation, and pyrosequencing can reliably detect DNA methylation differences among different cell populations, because bisulfite-treated DNA need not be cloned into bacterial expression vectors to avoid false positive results caused by random selection of clones. The corresponding selected hypermethylated CG sites in the si-NC group from the above four genes were validated through pyrosequencing. In summary, from the BSP and pyro-sequencing results, we find that only the CG dinucleotide locus at site 2 of the *IFN-γ* CG sites in the DMR region was confirmed to be significantly differentially methylated. The fact that the sequencing results were

419 not consistent with the MeDIP-Seq results may possibly be because the MeDIP-seq
420 enriched DNA sequences were sequence tandem repeats, which can be
421 immunoprecipitated by 5-mC antibody, causing false positive results. The middle
422 three CpG sites of the *IFN-γ* enriched DNA sequences could not be successfully
423 sequenced for the same reason. On the other hand, as BSP sequencing required the
424 cloning of bisulfite-treated DNA into bacterial expression vectors, and then randomly
425 select positive clones for subsequent PCR and sequencing. However, the number of
426 five clones selected by BSP sequencing in this study is relatively small and there is a
427 great chance, so we think that BSP results may not represent the actual level of
428 methylation. Bisulfite pyrosequencing, because of its own limitations on the length of
429 sequencing fragments, is based on the results of BSP sequencing to select each gene
430 difference CG site for pyrosequencing verification. The other three genes, *Cd24a,*
431 *TNF-α,* and *Lrrk2* pyrosequencing showed no significant methylation differences at
432 CG loci (S6-8 Fig), which may be due to the above reasons. Therefore, our data
433 suggest that lncRNA *Dnmt3aos* regulates *Dnmt3a* expression leading to aberrant
434 DNA methylation in macrophage polarization and *Dnmt3aos* specifically regulates
435 the DNA methylation patterns of genes. In addition, mechanisms by which *IFN-γ*
436 activates genes to promote macrophage activation via the Jak-STAT1 signaling
437 pathway are well studied. A recent study has indicated that *IFN-γ* suppresses the basal
438 expression of genes corresponding to an M2-like phenotype in *IFN-γ*-primed human
439 macrophages [49]. In view of this, our study did not further explore the *IFN-γ*
440 function in macrophage polarization.

In summary, this present study has determined the expression profiles of lncRNAs in macrophage polarization and contributes to the growing understanding of the role of lncRNAs in macrophage exposure to different stimuli. We found that *Dnmt3aos* plays a vital role in macrophage polarization. We also examined the global DNA methylation profiles between the si-NC and si-Dnmt3aos-transfected M(IL-4) macrophages, and demonstrated that *Dnmt3aos-Dnmt3a* axis-mediated aberrant DNA methylation may play a key role in regulating macrophage polarization. Our study enriches our understanding of the mechanism of macrophage polarization.

Materials and Methods

Ethics statement

All animal experimental procedures were approved by the Animal Ethics Committee of Wannan Medical College (Wuhu, China) and were performed according to the guidelines for the Care and Use of Laboratory Animals (Ministry of Health, China, 1998). The animals were sacrificed by cervical dislocation following anesthetized with a mixture of isoflurane and oxygen (3% v/v). All efforts were made to minimize the suffering of the animals.

Animals

BALB/c mice 6-10 weeks of age and 25-30 g in weight were purchased from the Experimental Animal Center of Qinglongshan (Nanjing, China), were housed in pathogen-free mouse colonies, and fed a chow diet. Mice were kept in 12 – 12 hours

463 of light-dark cycle; food and water were available ad libitum.

464

465 **Primary BMDM Isolation and Culture**

466 Primary bone marrow-derived macrophages (BMDMs) of mice were obtained as
467 described previously [22,23]. Briefly, BMDMs isolated from the femurs and tibias of
468 mice were cultured with DMEM supplemented with 20% fetal bovine serum (FBS,
469 Gibco), together with 20% L929 cell supernatant on 10 cm cell culture dishes at 37°C
470 and 5% CO_2. After 7 days of culture, the medium was removed, and the cells were
471 cultured in fresh RPMI-1640 supplemented with 10% FBS for an additional 24 h. To
472 induce the polarization of macrophages, BMDMs were then treated with DMEM/10%
473 FBS containing 100 ng/ml LPS (Sigma) and 20 ng/ml IFN-γ (PeproTech) to produce
474 M(LPS+IFN-γ) polarization, or with 20 ng/ml IL-4 (PeproTech) to produce M(IL-4)
475 macrophages. After 48 h stimulation, the resulting cells were harvested for
476 identification by morphology observation and flow cytometry (FCM) assay as in our
477 previous publication [22-24].

478

479 **Microarray and Bioinformatic Analyses**

480 An SBC mouse (4*180K) LncRNA microarray was designed for the global profiling
481 of mouse LncRNAs and protein-coding transcripts. The sample preparation and
482 microarray hybridization were performed as we have described previously [22].
483 Briefly, the total RNA from each sample was amplified and labeled by using a Low
484 Input Quick Amp WT Labeling kit (Agilent Technologies). Labeled cRNA was

purified using an RNeasy Mini kit (Qiagen GmbH). The concentration and specific activity of the labeled cRNAs (pmol Cy3/μg cRNA) were measured using a NanoDrop 2000. Each SBC mouse (4*180K) LncRNA microarray slide (Agilent Technologies Inc.) was hybridized with 1.65 μg Cy3-labeled cRNA using a gene expression hybridization kit (Agilent Technologies, Inc.). After 17 h of hybridization, the slides were scanned using an Agilent Microarray Scanner G2565C (Agilent Technologies, Inc.). Approximately 33,231 lncRNAs and 39,430 coding transcripts collected from the most authoritative databases, such as NCBI RefSeq, UCSC, ENSEMBL, FANTOM, UCR, and LNCRNA-DB were detected using microarrays. The Agilent Feature Extraction software (version 10.7; Agilent Technologies, Inc.) was used to analyze the acquired array images. Quantile normalization and subsequent data processing were performed using GeneSpring software version 11.0 (Agilent Technologies, Inc.). Microarray analysis was performed by Shanghai Biotechnology Corporation (Shanghai, China). Array data of differentially expressed protein-coding genes (fold change > 2 and $P < 0.5$) were deposited at the Gene Expression Omnibus database of the National Center for Biotechnology Information (accession no. GSE81922).

Isolation of RNA and RT-qPCR

Total RNAs were extracted using the TRIzol reagent (Invitrogen). Cytosolic and nuclear fractions were prepared using the PARIS™ Kit (ThermoFisher Scientific) according to the instructions, and cDNA was synthesized using a SuperScript III

First-Strand synthesis system (Life Technologies) with oligo(dT) and random primers according to the manufacturer's instructions. Quantitative RT-qPCR was performed using QuantiTect SYBR®-Green PCR kits (Qiagen) and glyceraldehyde 3-phosphate dehydrogenase (*GAPDH*) or U6 as an internal control utilizing an Applied Biosystems Q3 real-time PCR system. The reactions were incubated in 96-well plates at 95˚C for 3 min, followed by 40 cycles of 95˚C for 15 sec and 60˚C for 30 sec, followed by a dissociation curve. All the PCR reactions were run in triplicate. A complete list of primers used in this study is listed in Supplementary Table S1.

RNA FISH

RNA FISH was performed as described by the manufacturer's instructions as well as a previous publication [50]. In this study, a FAM-labeled locked nucleic acid (LNA) probe (Exiqon) against Dnmt3aos was used for RNA FISH. DAPI was used for nucleic counterstaining. Briefly, cultured cells were rinsed once with PBS and fixed with 4% paraformaldehyde (Sigma) in PBS for 20 min, then rinsed three times with PBS, permeabilized with 0.2% Triton X-100 (Sigma) in PBS for 15 min, washed twice with PBS, and incubated 30 min at 37°C with pre-hybridization buffer. Following this, cells were incubated 17 h at 37°C with hybridization buffer containing 500 nM FAM-labeled LNA probe. After successively washing with 4× SSC containing 0.5% Tween-20 three times, and 2× SSC, 1× SSC, and PBS once each, cells were stained with DAPI to visualize cell nuclei, rinsed three times with PBS, dried, and mounted in Vectashield mounting medium for fluorescent imaging. All

529 immunofluorescence staining was photographed under either a confocal or an
530 immunofluorescence microscope.
531
532 **Small Interfering RNA and Transfection of BMDMs**
533 LncRNA smart silencer (a siRNA mix containing three ASOs and three siRNAs)
534 targeting Dnmt3aos at different sites and small interfering RNAs (siRNAs) against
535 Dnmt3a and negative control (NC) with no definite target were synthesized by
536 RiboBio (Guangzhou, China). BMDMs were seeded on six-well plates at a density of
537 5×10^5 cells/well overnight and then transfected with siRNA or the negative control
538 at a final concentration of 100 nM using Lipofectamine 3000 (Invitrogen, USA). The
539 interfering efficiency was detected by RT-qPCR or western blot 48 hours after
540 transfection, and the siRNAs with silencing efficacy of more than 70% were selected
541 for further experiments. Sequences of siRNAs are provided in Supplementary Table
542 S2.
543
544 **Western blotting**
545 BMDMs were transfected with either siRNA or the negative control as described
546 above. At 48 h after transfection, cells were lysed in RIPA lysis buffer supplemented
547 with cocktail protease inhibitor (Roche). Proteins were separated by SDS-PAGE and
548 transferred onto a nitrocellulose filter membrane (Millipore, USA). The membranes
549 were incubated with primary antibodies, either anti-Dnmt3a (1:1000, Abcam, USA),
550 or anti-actin (1:1000, Santa Cruz, USA) in 5% milk/TBST buffer (25 mM Tris pH 7.4,

551 150 mM NaCl, 2.5 mM KCl, 0.1% Tween-20) overnight, followed by incubation with
552 horseradish peroxidase (HRP)-conjugated anti-mouse or anti-rabbit IgG (Abcam) for
553 1 h. The target proteins were detected on the membranes by enhanced
554 chemiluminescence (Millipore).
555
556 **Griess assay**
557 Primary BMDMs were transfected with si-NC or si-Dnmt3aos for 48 h, followed by
558 stimulation with LPS (100 ng/mL) plus IFN-γ (20 ng/ml) for an additional 6 h. The
559 supernatants from the two groups of cells were collected, and then 50 μl aliquots of
560 the conditioned medium were mixed with 50 μl of Griess reagent (Beyotime
561 Biotechnology, China) and incubated for 10 min at room temperature in the dark. The
562 colorimetric reaction was then measured at 540 nm using a Multiskan Go microplate
563 reader (Thermo Scientific, Rockford, IL, USA).
564
565 **Arginase activity assay**
566 Primary BMDMs were transfected with si-NC or si-Dnmt3aos for 48 h, followed by
567 stimulation with IL-4 (20 ng/ml) for an additional 24 h. Briefly, 1×10^6 treated
568 macrophages were lysed with 50 μl of 0.1% Triton X-100 for 30 min and then added
569 to 50 μl of 50 mM Tris-HCl/10 mM $Cl_2Mn \cdot 4H_2O$ (pH 7.5) and incubated at 55°C for
570 10 min. L-arginine hydrolysis was carried out by incubating with 25 μl of 0.5 M
571 L-arginine (pH 9.7) at 37°C for 60 min. The reaction was then stopped with 400 μl of
572 stop solution (H_2SO_4 (96%)/H_3PO_4 (85%)/H_2O (1:3:7, v/v/v)) and 25 μl of 9% of

573 2-isonitrosopropiophenone. The reactions were incubated at 100°C for 45 min and
574 100 μl of each sample was analyzed using a microplate reader at 540 nm. A standard
575 curve was generated from urea solutions (0-20 mM), which were used to determine
576 the final concentrations.

577

578 **Methylation Analysis by MeDIP Sequencing**

579 DNA and RNA from the si-NC and si-Dnmt3aos-transfected M(IL-4) macrophages
580 were extracted, and high throughput sequencing and MeDIP-seq were conducted by
581 Shanghai Biotechnology Corporation, China. Detailed procedures were according to
582 Chavez's publication [51]. Briefly, DNA (3 μg) was sonicated at intensity 4 for 200
583 cycles per burst for 55 s (Covaris S2), and DNA fragments were end-repaired,
584 ATP-tailed, and adapter-ligated with the Sample Preparation Kit (Illumina). Then
585 DNA was recovered by AMPure XP Beads and used for methylated DNA
586 immunoprecipitation (MeDIP) using the Magnetic Methylated DNA
587 Immunoprecipitation Kit (Diagenode) according to the manufacturer's protocol. After
588 MeDIP, remaining DNA was PCR-amplified with sequencing primers and used for
589 sequencing (Illumina Hiseq2500). Raw reads were preprocessed using the
590 FASTX-Toolkit. MeDIP-seq peaks were counted using MACS. The depth of genomic
591 regions was calculated and plotted using Integrative Genomics Viewer (IGV) and
592 IGV Tools software.

593

594 **Bisulfite modification, bisulfite sequencing, and pyrosequencing**

595 Genomic DNA was isolated from the si-NC and si-Dnmt3aos-transfected M(IL-4)
596 macrophage cells and was then treated with bisulfite using the Imprint DNA
597 Modification Kit (Sigma-Aldrich). Bisulfite sequencing and pyrosequencing were
598 conducted by Shanghai Sangon Biotech Corporation, China. The procedure details
599 were reported in previous publications [51,52]. Briefly, the bisulfite conversion-based
600 PCR primers were designed with the MethPrimer program. Primers are listed in
601 Supplementary Table S3. PCR was performed using P*fu* DNA polymerase (Sangon
602 Biotech Corporation) under the following conditions: initial incubation at 98˚C for 4
603 min, then 20 cycles of 94˚C for 45 s, 66˚C for 45 s, and 72˚C for 1 min of touchdown
604 PCR with a decrease of 0.5˚C every cycle, continuing with 20 cycles of 94˚C for 45 s,
605 56˚C for 45 s, and 72˚C for 1 min, followed by 72˚C for 8 min for the gene promoter.
606 The PCR products were purified using the Wizard DNA Clean-up System (Promega),
607 and then cloned into the pGEM-T Easy Vector I (Promega). Five independent clones
608 for each sample were picked, and the T7 and Sp6 primers were used to sequence
609 inserted fragments. As for pyrosequencing, biotinylated DNA fragments (about 5
610 pmoles each) were attached to streptavidin-modified paramagnetic beads
611 (Dynabeads™ M-280, Dynal A/S, Skøyen, Norway) by slow revolution of the
612 suspensions in a thermostated (43° C) chamber (HB-1, Techne Ltd, Duxford, England)
613 in a high salt (BW) buffer (0.05% Tween 20, 0.5 mm EDTA, 1 m NaCl, 5 mm
614 Tris-HCl, pH 7.6). Following washing steps in BW buffer and 10 mm Tris-HAc, pH
615 7.6, the material was resuspended in 0.15 M NaOH. After a 10-min incubation period,
616 the separated DNA strands were saved for subsequent processing as follows: beads

were washed twice in 10 mm Tris-HAc, pH 7.6 and transferred to a solution (20 mm $Mg(CH_3COO)_2$, 10 mm Tris-HAc pH 7.6), containing 20-25 pmoles of the appropriate sequencing primer (primers are listed in Supplementary Table S4). Subsequently, the annealing procedure was conducted. This step comprised heating for 45 s at 95° C followed by cooling at room temperature. Throughout most of the preparation steps, the bead-coupled fragments were processed in parallel using a manifold device equipped with 96 magnetic ejectable microcylinders (PSQ 96 Sample Prep Tool, Pyrosequencing AB), which were protected by a disposable plastic pocketed cover. DNA sequence reading was conducted in a P3 PSQ 96 instrument (Pyrosequencing AB).

Statistical Analyses

Descriptive statistics were generated for all quantitative data with presentation of means and S.D. Statistical analysis was carried out using Prism (GraphPad) software. Student's *t* test was used to determine statistical significance, defined as $P < 0.05$.

Acknowledgments

This project was supported by the National Natural Science Foundation of China (grant nos. 81472017, 81701557, 81802503, 81870017, and 81772180), Key Projects of Natural Science Research of Universities in Anhui Province (grant no. KJ2016A721 and KJ2018A0265). We thank LetPub (www.letpub.com) for its linguistic assistance during the preparation of this manuscript.

639

640 **Author Contributions**

641 K. L. and Y. Z. designed the study. X. L. wrote the paper. M. Z. performed BMDM
642 cells isolation and culture. H. Y. performed western blotting experiments. X. L.
643 performed the other all experiments. X. K., W. P., Y. X., X. Z. and T. C. analyzed the
644 data. M. Z. and J. Y. contributed reagents/materials and animal housekeeping. All
645 authors approved the final version of the manuscript.

646

647 **Competing interests**

648 The authors declare no competing interests.

649

650 **References**

651 1. Lawrence T, Natoli G. Transcriptional regulation of macrophage polarization:
652 enabling diversity with identity. Nat Rev Immunol. 2011; 11(11):750-61.
653 https://doi.org/10.1038/nri3088 PMID: 22025054.
654 2. Ruffell B, Affara NI, Coussens LM. Differential macrophage programming in the
655 tumor microenvironment. Trends Immunol. 2012;
656 33(3):119-26. https://doi.org/10.1016/j.it.2011.12.001 PMID: 22277903; PubMed
657 Central PMCID: PMCPMC3294003.
658 3. Murray PJ, Wynn TA. Obstacles and opportunities for understanding macrophage
659 polarization. J Leukoc Biol. 2011; 89(4):557-63.
660 https://doi.org/10.1189/jlb.0710409 PMID: 21248152; PubMed Central PMCID:

661 PMCPMC3058818.

662 4. Martinez FO, Gordon S, Locati M, Mantovani A. Transcriptional profiling of the
663 human monocyte-to-macrophage differentiation and polarization: new molecules
664 and patterns of gene expression. J Immunol. 2006; 177(10):7303-11.
665 https://doi.org/10.4049/jimmunol.177.10.7303 PMID: 17082649.

666 5. Labonte AC, Tosello-Trampont AC, Hahn YS. The role of macrophage
667 polarization in infectious and inflammatory diseases. Mol Cells. 2014;
668 37(4):275–85. https://doi.org/10.14348/molcells.2014.2374 PMID: 24625576;
669 PubMed Central PMCID: PMCPMC4012075.

670 6. Buscher K, Ehinger E, Gupta P, Pramod AB, Wolf D, Tweet G, et al. Natural
671 variation of macrophage activation as disease-relevant phenotype predictive of
672 inflammation and cancer survival. Nat Commun. 2017; 8:ncomms16041.
673 https://doi.org/10.1038/ncomms16041 PMID: 28737175; PubMed Central
674 PMCID: PMCPMC5527282.

675 7. Olefsky JM, Glass CK. Macrophages, inflammation, and insulin resistance. Annu
676 Rev Physiol. 2010; 72:219-46.
677 https://doi.org/ 10.1146/annurev-physiol-021909-135846 PMID: 20148674.

678 8. Wang X, Cao Q, Yu L, Shi H, Xue B. Epigenetic regulation of macrophage
679 polarization and inflammation by DNA methylation in obesity. Jci Insight. 2016;
680 1(19):e87748. https://doi.org/10.1172/jci.insight.87748 PMID: 27882346;
681 PubMed Central PMCID: PMCPMC5111504.

682 9. Guttman M, Amit I, Garber M, French C, Lin MF, Feldser D, et al. Chromatin

683 signature reveals over a thousand highly conserved large non-coding RNAs in
684 mammals. Nature. 2009; 458(7235):223-7. https://doi.org/10.1038/nature07672
685 PMID: 19182780; PubMed Central PMCID: PMCPMC2754849.
686 10. Carpenter S, Aiello D, Atianand MK, Ricci EP, Gandhi P, Hall LL, et al. A long
687 noncoding RNA mediates both activation and repression of immune response
688 genes. Science. 2013; 341(6147):789-92. https://doi.org/10.1126/science.1240925
689 PMID: 23907535; PubMed Central PMCID: PMCPMC4376668.
690 11. Chen MT, Lin HS, Shen C, Ma YN, Wang F, Zhao HL, et al. PU.1-regulated long
691 noncoding RNA lnc-MC controls human monocyte/macrophage differentiation
692 through interaction with microRNA 199a-5p. Mol Cell Biol. 2015;
693 35(18):3212-24. https://doi.org/10.1128/MCB.00429-15 PMID: 26149389;
694 PubMed Central PMCID: PMCPMC4539372.
695 12. Mao AP, Shen J, Zuo Z. Expression and regulation of long noncoding RNAs in
696 TLR4 signaling in mouse macrophages. BMC Genomics. 2015; 16:45.
697 https://doi.org/10.1186/s12864-015-1270-5 PMID: 25652569; PubMed Central
698 PMCID: PMCPMC4320810.
699 13. Reddy MA, Chen Z, Park JT, Wang M, Lanting L, Zhang Q, et al. Regulation of
700 inflammatory phenotype in macrophages by a diabetes-induced long noncoding
701 RNA. Diabetes. 2014; 63(12):4249-61. https://doi.org/10.2337/db14-0298 PMID:
702 25008173; PubMed Central PMCID: PMCPMC4238007.
703 14. Huang Z, Luo Q, Yao F, Qing C, Ye J, Deng Y, et al. Identification of
704 differentially expressed long non-coding RNAs in polarized macrophages. Sci

Rep. 2016; 6:19705. https://doi.org/10.1038/srep19705 PMID: 26796525; PubMed Central PMCID: PMCPMC4726337.

15. Yang X, Wang X, Liu D, Yu L, Xue B, Shi H. Epigenetic regulation of macrophage polarization by DNA methyltransferase 3b. Mol Endocrinol. 2014; 28(4):565-74. https://doi.org/10.1210/me.2013-1293 PMID: 24597547; PubMed Central PMCID: PMCPMC3968399.

16. Suzuki MM, Bird A. DNA methylation landscapes: provocative insights from epigenomics. Nat Rev Genet. 2008; 9(6):465-76. https://doi.org/10.1038/nrg2341 PMID: 18463664.

17. Maunakea AK, Chepelev I, Zhao K. Epigenome mapping in normal and disease states. Circ Res. 2010; 107(3):327-39. https://doi.org/10.1161/CIRCRESAHA.110.222463 PMID: 20689072; PubMed Central PMCID: PMCPMC2917837.

18. Backdahl L, Bushell AS. Inflammatory signalling as mediator of epigenetic modulation in tissue-specific chronic inflammation. Int J Biochem Cell Biol. 2009; 41(1):176-84. https://doi.org/10.1016/j.biocel.2008.08.023 PMID: 18793748.

19. Takeuch O, Akira S. Epigenetic control of macrophage polarization. Eur J Immunol. 2011; 41(9):2490-3. https://doi.org/10.1002/eji.201141792 PMID: 21952803.

20. Satoh T, Takeuchi O, Vandenbon A, Yasuda K, Tanaka Y, Kumagai Y, et al. The Jmjd3-Irf4 axis regulates M2 macrophage polarization and host responses against helminth infection. Nat Immunol. 2010; 11(10):936-44.

https://doi.org/10.1038/ni.1920 PMID: 20729857.

21. Miller SA, Mohn SE, Weinmann AS. Jmjd3 and UTX play a demethylase-independent role in chromatin remodeling to regulate T-box family member-dependent gene expression. Mol Cell. 2010; 40(4):594-605. https://doi.org/10.1016/j.molcel.2010.10.028 PMID: 21095589; PubMed Central PMCID: PMCPMC3032266.

22. Jiang L, Li X, Zhang Y, Zhang M, Tang Z, Lv K. Microarray and bioinformatics analyses of gene expression profiles in BALB/c murine macrophage polarization. Mol Med Rep. 2017; 16(5):7382-7390. https://doi.org/10.3892/mmr.2017.7511 PMID: 28944843; PubMed Central PMCID: PMCPMC5865869.

23. Zhang Y, Zhang Y, Li X, Zhang M, Lv K. Microarray analysis of circular RNA expression patterns in polarized macrophages. Int J Mol Med. 2017; 39(2):373-379. https://doi.org/10.3892/ijmm.2017.2852 PMID: 28075448; PubMed Central PMCID: PMCPMC5358696.

24. Zhang Y, Zhang M, Zhong M, Suo Q, Lv K. Expression profiles of miRNAs in polarized macrophages. Int J Mol Med. 2013; 31(4):797-802. https://doi.org/10.3892/ijmm.2013.1260 PMID: 23443577.

25. Ørom UA, Derrien T, Beringer M, Gumireddy K, Gardini A, Bussotti G, et al. Long noncoding RNAs with enhancer-like function in human cells. Cell. 2010; 143(1):46-58. https://doi.org/10.1016/j.cell.2010.09.001 PMID: 20887892; PubMed Central PMCID: PMCPMC4108080.

26. Tsai MC, Manor O, Wan Y, Mosammaparast N, Wang JK, Lan F, et al. Long

749 noncoding RNA as modular scaffold of histone modification complexes. Science.
750 2010; 329(5992):689-93. https://doi.org/10.1126/science.1192002 PMID:
751 20616235; PubMed Central PMCID: PMCPMC2967777.
752 27. Rinn JL, Kertesz M, Wang JK, Squazzo SL, Xu X, Brugmann SA, et al.
753 Functional demarcation of active and silent chromatin domains in human loci by
754 noncoding RNAs. Cell. 2007; 129(7):1311-23.
755 https://doi.org/10.1016/j.cell.2007.05.022 PMID: 17604720; PubMed Central
756 PMCID: PMCPMC2084369.
757 28. Chan J, Atianand M, Jiang Z, Carpenter S, Aiello D, Elling R, et al. Cutting edge:
758 a natural antisense transcript, AS-IL1α, controls inducible transcription of the
759 proinflammatory cytokine IL-1α. J Immunol. 2015; 195(4):1359-63.
760 https://doi.org/10.4049/jimmunol.1500264 PMID: 26179904; PubMed Central
761 PMCID: PMCPMC4530055.
762 29. Qin W, Li X, Xie L, Li S, Liu J, Jia L, et al. A long non-coding RNA, APOA4-AS,
763 regulates APOA4 expression depending on HuR in mice. Nucleic Acids Res. 2016;
764 44(13):6423-33. https://doi.org/10.1093/nar/gkw341 PMID: 27131369; PubMed
765 Central PMCID: PMCPMC5291254.
766 30. Gong C, Li Z, Ramanujan K, Clay I, Zhang Y, Lemire-Brachat S, et al. A long
767 non-coding RNA, LncMyoD, regulates skeletal muscle differentiation by blocking
768 IMP2-mediated mRNA translation. Dev Cell. 2015; 34(2):181-91.
769 https://doi.org/10.1016/j.devcel.2015.05.009 PMID: 26143994.
770 31. Faghihi MA, Modarresi F, Khalil AM, Wood DE, Sahagan BG, Morgan TE, et al.

771 Expression of a noncoding RNA is elevated in Alzheimer's disease and drives
772 rapid feed-forward regulation of β-secretase. Nat Med. 2008; 14(7):723-30.
773 https://doi.org/10.1038/nm1784 PMID: 18587408; PubMed Central PMCID:
774 PMCPMC2826895.
775 32. Wang L, Zhao Y, Bao X, Zhu X, Kwok YK, Sun K, et al. LncRNA Dum interacts
776 with Dnmts to regulate Dppa2 expression during myogenic differentiation and
777 muscle regeneration. Cell Res. 2015; 25(3):335-50.
778 https://doi.org/10.1038/cr.2015.21 PMID: 25686699; PubMed Central PMCID:
779 PMCPMC4349245.
780 33. Brenner C, Deplus R, Didelot C, Loriot A, Viré E, De Smet C, et al. Myc
781 represses transcription through recruitment of DNA methyltransferase corepressor.
782 EMBO J. 2014; 24(2):336-46. https://doi.org/10.1038/sj.emboj.7600509 PMID:
783 15616584; PubMed Central PMCID: PMCPMC545804.
784 34. Xu J, Wang YY, Dai YJ, Zhang W, Zhang WN, Xiong SM, et al. DNMT3A
785 Arg882 mutation drives chronic myelomonocytic leukemia through disturbing
786 gene expression/DNA methylation in hematopoietic cells. Proc Natl Acad Sci U S
787 A. 2014; 111(7):2620-5. https://doi.org/10.1073/pnas.1400150111 PMID:
788 24497509; PubMed Central PMCID: PMCPMC3932885.
789 35. Zhang G, Estève PO, Chin HG, Terragni J, Dai N, Corrêa IR Jr, et al. Small
790 RNA-mediated DNA (cytosine-5) methyltransferase 1 inhibition leads to aberrant
791 DNA methylation. Nucleic Acids Res. 2015; 43(12):6112-24.
792 https://doi.org/10.1093/nar/gkv518 PMID: 25990724; PubMed Central PMCID:

PMCPMC4499142.

36. Sandoval J, Heyn H, Moran S, Serra-Musach J, Pujana MA, Bibikova M, et al. Validation of a DNA methylation microarray for 450,000 CpG sites in the human genome. Epigenetics. 2016; 6(6):692-702. PMID: 21593595.

37. Li K, Xu W, Guo Q, Jiang Z, Wang P, Yue Y, et al. Differential macrophage polarization in male and female BALB/c mice infected With coxsackievirus B3 defines susceptibility to viral myocarditis. Circ Res. 2009; 105(4):353-64. https://doi.org/10.1161/CIRCRESAHA.109.195230 PMID: 19608981.

38. Chacón-Salinas R, Serafín-López J, Ramos-Payán R, Méndez-Aragón P, Hernández-Pando R, Van Soolingen D, et al. Differential pattern of cytokine expression by macrophages infected in vitro with different Mycobacterium tuberculosis genotypes. Clin Exp Immunol. 2005; 140(3):443-9. https://doi.org/10.1111/j.1365-2249.2005.02797.x PMID: 15932505; PubMed Central PMCID: PMCPMC1809389.

39. Verreck FA, de Boer T, Langenberg DM, van der Zanden L, Ottenhoff TH. Phenotypic and functional profiling of human proinflammatory type-1 and anti-inflammatory type-2 macrophages in response to microbial antigens and IFN-gamma- and CD40L-mediated costimulation. J Leukoc Biol. 2006; 79(2):285-93. https://doi.org/10.1189/jlb.0105015 PMID: 16330536.

40. Samuel VT, Shulman GI. Mechanisms for insulin resistance: common threads and missing links. Cell. 2012; 148(5):852-71. https://doi.org/10.1016/j.cell.2012.02.017 PMID: 22385956; PubMed Central

PMCID: PMCPMC3294420.

41. Zhou YX, Zhao W, Mao LW, Wang YL, Xia LQ, Cao M, et al. Long non-coding RNA NIFK-AS1 inhibits M2 polarization of macrophages in endometrial cancer through targeting miR-146a. Int J Biochem Cell Biol. 2018; 104:25-33. https://doi.org/10.1016/j.biocel.2018.08.017 PMID: 30176290.

42. Zhao JL, Huang F, He F, Gao CC, Liang SQ, Ma PF, et al. Forced activation of notch in macrophages represses tumor growth by upregulating miR-125a and disabling tumor-associated macrophages. Cancer Res. 2016; 76(6):1403-15. https://doi.org/10.1158/0008-5472.CAN-15-2019 PMID: 26759236.

43. Zhang Y, Zhang M, Li X, Tang Z, Wang X, Zhong M, et al. Silencing microRNA-155 attenuates cardiac injury and dysfunction in viral myocarditis via promotion of M2 phenotype polarization of macrophages. Sci Rep. 2016; 6:22613. https://doi.org/10.1038/srep22613 PMID: 26931072; PubMed Central PMCID: PMCPMC4773853.

44. Haney SL, Upchurch GM, Opavska J, Klinkebiel D, Hlady RA, Suresh A, et al. Promoter hypomethylation and expression is conserved in mouse chronic lymphocytic leukemia induced by decreased or inactivated Dnmt3a. Cell Rep. 2016; 15(6):1190-201. https://doi.org/10.1016/j.celrep.2016.04.004 PMID: 27134162; PubMed Central PMCID: PMCPMC4864108.

45. Shikauchi Y, Saiura A, Kubo T, Niwa Y, Yamamoto J, Murase Y, et al. SALL3 interacts with DNMT3A and shows the ability to inhibit CpG island methylation in hepatocellular carcinoma. Mol Cell Biol. 2009; 29(7):1944-58.

837 https://doi.org/10.1128/MCB.00840-08 PMID: 19139273; PubMed Central
838 PMCID: PMCPMC2655625.
839 46. Feng S, Jacobsen SE, Reik W. Epigenetic reprogramming in plant and animal
840 development. Science. 2010; 330(6004):622-7.
841 https://doi.org/10.1126/science.1190614 PMID: 21030646; PubMed Central
842 PMCID: PMCPMC2989926.
843 47. Jones PA, Baylin SB. The epigenomics of cancer. Cell. 2007; 128(4):683-92.
844 https://doi.org/10.1016/j.cell.2007.01.029 PMID: 17320506; PubMed Central
845 PMCID: PMCPMC3894624.
846 48. Luczak MW, Jagodziński PP. The role of DNA methylation in cancer
847 development. Folia Histochem Cytobiol. 2006; 44(3):143-54. PMID: 16977793.
848 49. Kang K, Park SH, Chen J, Qiao Y, Giannopoulou E, Berg K, et al. Interferon-γ
849 represses M2 gene expression in human macrophages by disassembling enhancers
850 bound by the transcription factor MAF. Immunity. 2017; 47(2):235-250.
851 https://doi.org/10.1016/j.immuni.2017.07.017 PMID: 28813657; PubMed Central
852 PMCID: PMCPMC5568089.
853 50. Wang L, Bu P, Ai Y, Srinivasan T, Chen HJ, Xiang K, et al. A long non-coding
854 RNA targets microRNA miR-34a to regulate colon cancer stem cell asymmetric
855 division. Elife. 2016; 5 pii:e14620. https://doi.org/10.7554/eLife.14620 PMID:
856 27077950; PubMed Central PMCID: PMCPMC4859802.
857 51. Chavez L, Jozefczuk J, Grimm C, Dietrich J, Timmermann B, Lehrach H, et al.
858 Computational analysis of genome-wide DNA methylation during the

differentiation of human embryonic stem cells along the endodermal lineage. Genome Res. 2010; 20(10):1441-50. https://doi.org/10.1101/gr.110114.110 PMID: 20802089; PubMed Central PMCID: PMCPMC2945193.

52. Alderborn A, Kristofferson A, Hammerling U. Determination of single-nucleotide polymorphisms by real-time pyrophosphate DNA sequencing. Genome Res. 2000; 10(8):1249-58. https://doi.org/10.1101/gr.10.8.1249 PMID: 10958643; PubMed Central PMCID: PMCPMC310924.

Figure Legends:

Fig 1. Identification and characterization of *Dnmt3aos*. (a-b) LncRNA microarray expression data from BMDMs incubated in distinct polarizing conditions. A total of 1,251 differentially-expressed lncRNAs were identified between the M(LPS+IFN-γ) and M(IL-4) macrophages. **(a)** Scatter plots show the variation in lncRNA expression between the M(LPS+IFN-γ) and M(IL-4) macrophages. The values of the X and Y axes in the scatter plot are the averaged normalized values in each group (log2-scaled). **(b)** Heat maps of lncRNAs expression profiles between the two groups. "Red" indicates high relative expression and "green" indicates low relative expression. One ANOVA test was used for statistical analysis. LncRNA with expression fold change > 2 and with FDR-adjusted *P* value < 0.05 was considered statistically significant. **(c)** Confirmation of the differential expression of lncRNAs by RT-qPCR**.** Four differentially expressed lncRNAs were validated by RT-qPCR. The y-axis represents the log2-transformed median fold-change in expression. **(d)** LncRNA Dnmt3aos

881 locates on the Dnmt3a opposite strand on mouse chromosome 12. **(e)** RT-qPCR
882 detection of *Dnmt3aos* level in cellular fractions from BMDMs. U6 and GAPDH
883 were the nuclear and cytoplasmic controls, respectively. Data were expressed as the
884 means ± SD of three independent experiments. **(f)** *Dnmt3aos* expression in BMDMs
885 detected by RNA-FISH. Scale bar, 20 mm.

886 **Fig 2. Differential expression of *Dnmt3aos* during macrophage polarization. (a)**
887 *Dnmt3aos* was assessed by RT-qPCR and normalized to GAPDH in BMDMs after 48
888 h of stimulation with LPS (100 ng/ml) plus IFN-γ (20 ng/ml) or IL-4 (20 ng/ml). **(b)**
889 *Dnmt3aos* levels in macrophages following M(LPS+IFN-γ)-to-M(IL-4)
890 re-polarization by IL-4 (20 ng/ml) for 24 h. **(c)** *Dnmt3aos* levels in macrophages
891 following M(IL-4)-to-M(LPS+IFN-γ) re-polarization by LPS (100 ng/ml) plus IFN-γ
892 (20 ng/ml) for 8 h. Data are expressed as the means ± SD of three independent
893 experiments. $^{**}P < 0.01$, $^{***}P < 0.001$, *P*-value was calculated based on Student's *t*
894 test.

895 **Fig 3. *Dnmt3aos* regulates *Dnmt3a* mRNA and protein expression *in vitro*. (a-b)**
896 Time course of *Dnmt3aos* **(a)** or *Dnmt3a* **(b)** expression in BMDMs after stimulation
897 with LPS (100 ng/ml) plus IFN-γ (20 ng/ml) or IL-4 (20 ng/ml). **(c-d)** Knockdown of
898 *Dnmt3aos* **(c)** or *Dnmt3a* **(d)** in BMDMs with lncRNA smart silencer (si-Dnmt3aos)
899 or siRNA specifically targeting Dnmt3a (si-Dnmt3a). *Dnmt3aos* and *Dnmt3a*
900 expression were assessed by RT-qPCR. Nontargeting siRNA negative control (si-NC)
901 was used as the control. **(e)** Knockdown of *Dnmt3aos* in BMDMs with si-Dnmt3aos
902 or si-NC. Protein expression of *Dnmt3a* and *β-actin* set as the endogenous control

903 were measured by western blotting. Data are expressed as the means ± SD of two
904 independent experiments. $^{**}P < 0.01$, $^{***}P < 0.001$. *P*-value was calculated based on
905 Student's *t* test.

906 **Fig 4. *Dnmt3aos* plays important roles in BMDMs polarization. (a-b)** Primary
907 BMDMs were transfected with si-NC or si-Dnmt3aos for 48 h, followed by
908 stimulation with LPS (100 ng/mL) plus IFN-γ (20 ng/ml) for an additional 6 h. **(a)**
909 Supernatants from the two groups of cells were observed for NO production using
910 Griess activity assays. **(b)** RT-qPCR**.** RNA was extracted from the two groups of cells
911 and subjected to RT-qPCR analysis with primers specific to iNOS, TNF-α, and IL-12.
912 **(c-d)** Primary BMDMs were transfected with si-NC or si-Dnmt3aos for 48 h,
913 followed by stimulation with IL-4 (20 ng/ml) for an additional 24 h. **(c)** Cells were
914 lysed and investigated for urea production using arginase activity assays. **(d)**
915 RT-qPCR**.** RNA was extracted from the two groups of cells and subjected to
916 RT-qPCR analysis with primers specific to Arg1, YM1, and FIZZ1. GAPDH was set
917 as the endogenous control. Data are expressed as the means ± SD of three
918 independent experiments. $^{*}P < 0.05$, $^{**}P < 0.01$, $^{***}P < 0.001$. *P*-value was
919 calculated based on Student's *t* test.

920 **Fig 5. MeDIP-seq methylation profiles between the si-NC and si-Dnmt3aos**
921 **transfected M(IL-4) macrophages. (a)** Distribution and counts of CpG islands (CGI)
922 obtained from the **s**i-NC and si-Dnmt3aos transfected M(IL-4) macrophages are
923 shown in the histogram. **(b)** The average proportions of CGI obtained from the **s**i-NC
924 and si-Dnmt3aos-transfected M(IL-4) macrophages in each region defined by

925 genomic structure are shown in pie charts. Promoters (-2 kb regions around their
926 TSSs), CpG islands and their Shores (up/down stream 2 kb from the CpG island),
927 Shelf (up/down stream 2-4 kb from the CpG island), and Open Sea (more than 4 kb
928 from the CpG island). **(c)** Heat map of differentially methylated regions (DMRs),
929 selected by highest variances between samples, including mean rpm signals for the
930 two biological replicates of the **s**i-NC and si-Dnmt3aos-transfected M(IL-4)
931 macrophages. Red indicates up-regulated fold change and green indicates
932 down-regulated fold change. **(d)** Chromosomal distribution of DMRs. Red represents
933 high methylation and blue represents low methylation. The height represents logFC
934 (fold change). **(e)** Circos plot of global genomic methylation level across each
935 chromosome between the **s**i-NC and si-Dnmt3aos-transfected M(IL-4) macrophages.
936 The coverage of the genome is observed by a 100 K window, indicating the
937 methylation level of the genome; the outermost circle in the figure is the
938 chromosomes, and each circle inside indicates the genome methylation level of the
939 sample.

940 **Fig 6. Enrichment analysis of DMRs. (a-b)** Analysis of the top 30 GO enrichment
941 terms **(a)** and the top 30 KEGG pathway enrichment terms **(b)** of DMRs. For each
942 term, the expected and observed gene numbers along with the statistical significance
943 (q-value) for the enrichments are presented. **(c-d)** Correlation analysis of differentially
944 methylated region (DMR) methylation status of the **s**i-NC and
945 si-Dnmt3aos-transfected M(IL-4) macrophages and differentially expressed genes
946 (DEGs) of M(LPS+IFN-γ) and M(IL-4) macrophages. **(c)** Overall view of the

947 negative correlation between methylation and expression. DEGs are shown on the
948 longitudinal coordinates to show the difference in expression, and the difference in
949 methylation is shown on the transverse coordinates. **(d)** Heat map shows the level and
950 correlation of methylation and expression of each gene. The same genes were placed
951 on the same lines.

952 **Fig 7. The *Dnmt3aos-Dnmt3a* axis regulates macrophage polarization-related**
953 **gene expression through modification of DNA methylation. (a-b)** RT-qPCR
954 validation. Knockdown of *Dnmt3aos* **(a)** or *Dnmt3a* **(b)** expression in M(IL-4)
955 macrophages with lncRNA smart silencer (si-Dnmt3aos) or siRNA specifically
956 targeting Dnmt3a (si-Dnmt3a), respectively. M(IL-4) macrophage phenotype related
957 genes and the selected DMR-related genes obtained from negative correlation analysis
958 of DMRs located in promoter regions and DEGs. **(c)** M(IL-4) macrophages were
959 treated with the DNMT inhibitor 5-Aza-CdR for 72 h. The expression of the selected
960 DMRs (obtained from negative correlation analysis of DMRs located in promoter
961 regions and DEGs) were assessed by RT-qPCR. **(d)** The location and exhibition of
962 DNA sequences of DMRs in the promoter region of *IFN-γ* obtained from MeDIP-seq
963 enrichment. The CG sites (sites 1-2 and sites 6-8 in order) with underlining and red
964 color were successfully BSP sequenced. **(e-f)** *IFN-γ* methylation profiles in the **s**i-NC
965 or si-Dnmt3aos-transfected M(IL-4) macrophages. **(e)** The open and filled circles
966 symbolize the unmethylated and methylated CGs, respectively. Five colonies of
967 separate CG sites from each group were further analyzed by BSP sequencing. **(f)**
968 Pyrosequencing analysis of the CG methylation level in the selected CG sites of the

969 *IFN-γ* gene promoter from BSP sequencing results. The figure illustrates the variation
970 in methylation level at CG site 2 and site 7 in the **s**i-NC or si-Dnmt3aos-transfected
971 M(IL-4) macrophages. **(g)** The expression levels of *IFN-γ* mRNA in M(IL-4)
972 macrophages treated with 5-Aza-CdR, SGI-1027, Dnmt3aos lncRNA smart silencer
973 (si-Dnmt3aos), or Dnmt3a siRNA (si-Dnmt3a). Data were expressed as the means ±
974 SD of three independent experiments. **P* < 0.05. *P*-value was calculated based on
975 Student's *t* test.
976
977
978
979
980
981
982
983
984
985
986
987
988
989
990

991 **Fig 1.**

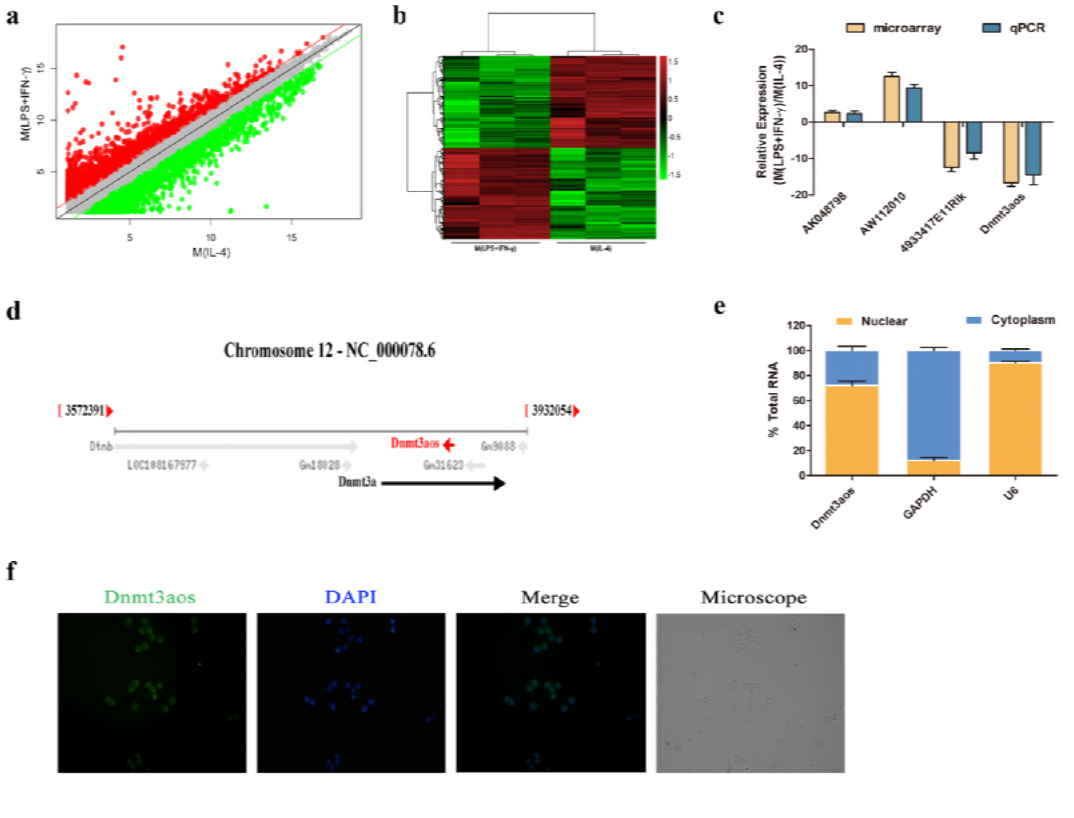

992

993

994 **Fig 2.**

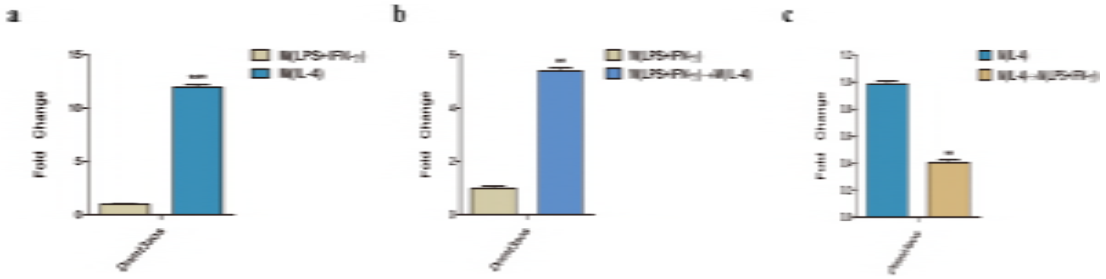

995

996

997

998

999

1000

Fig 3.

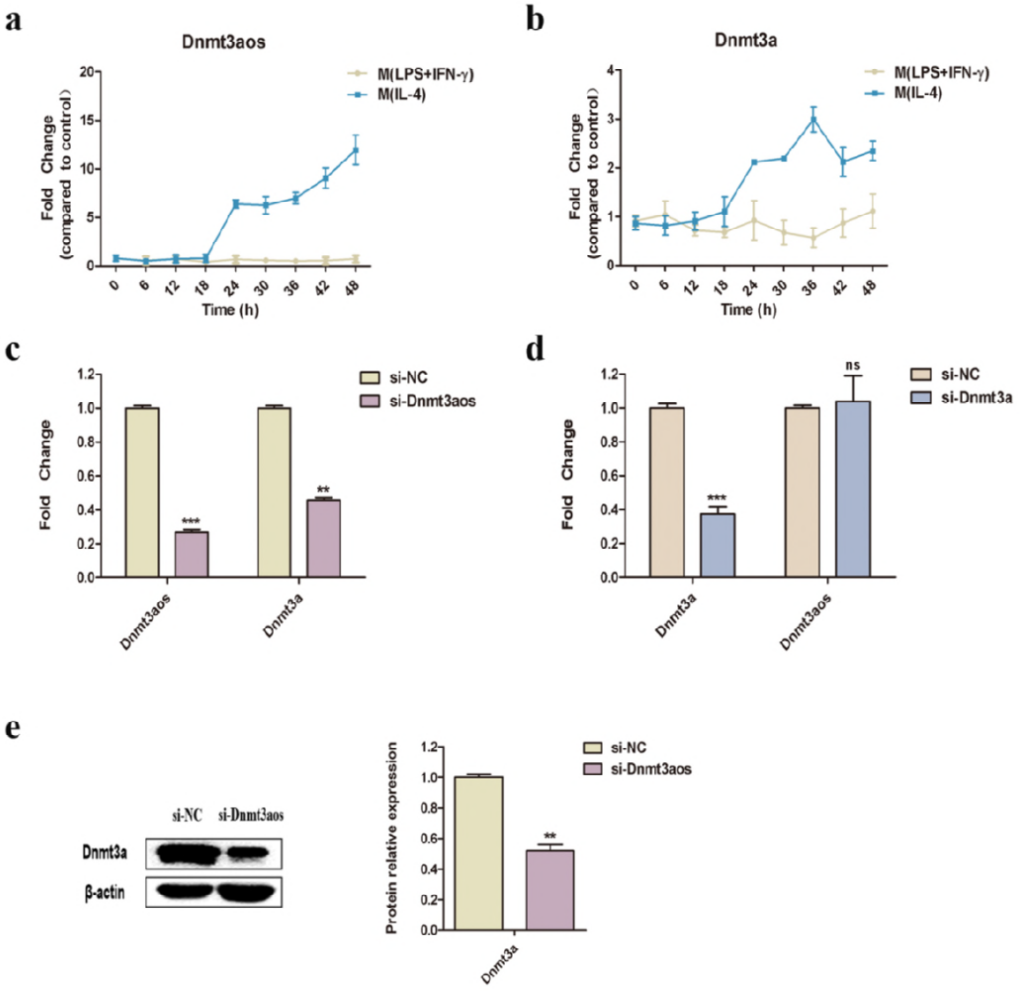

Fig 4.

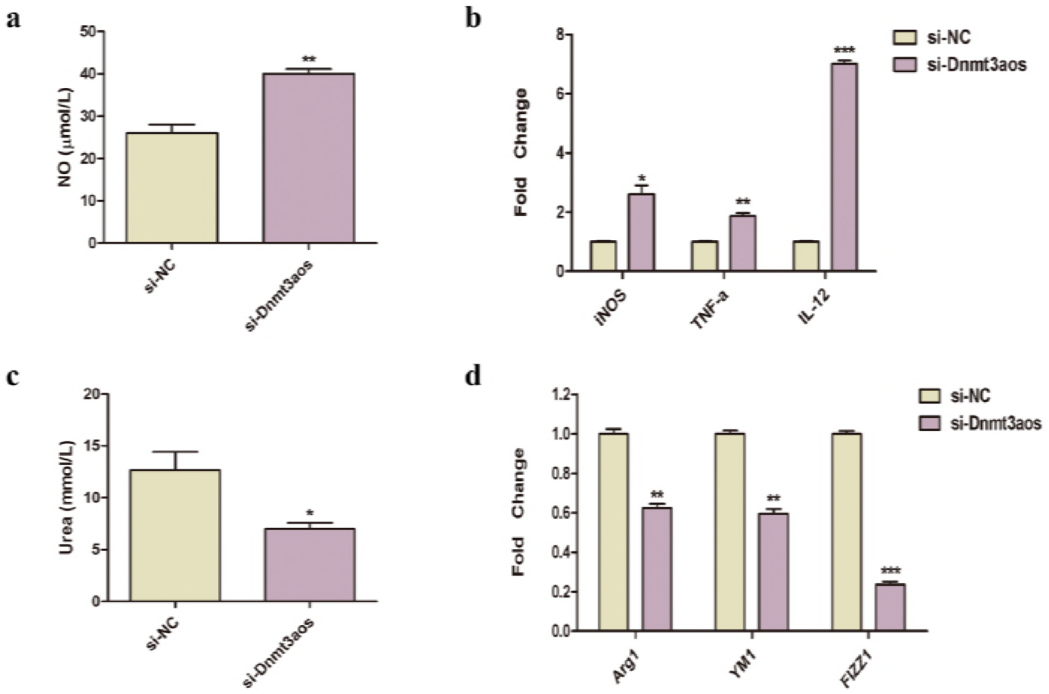

1026 **Fig 5.**

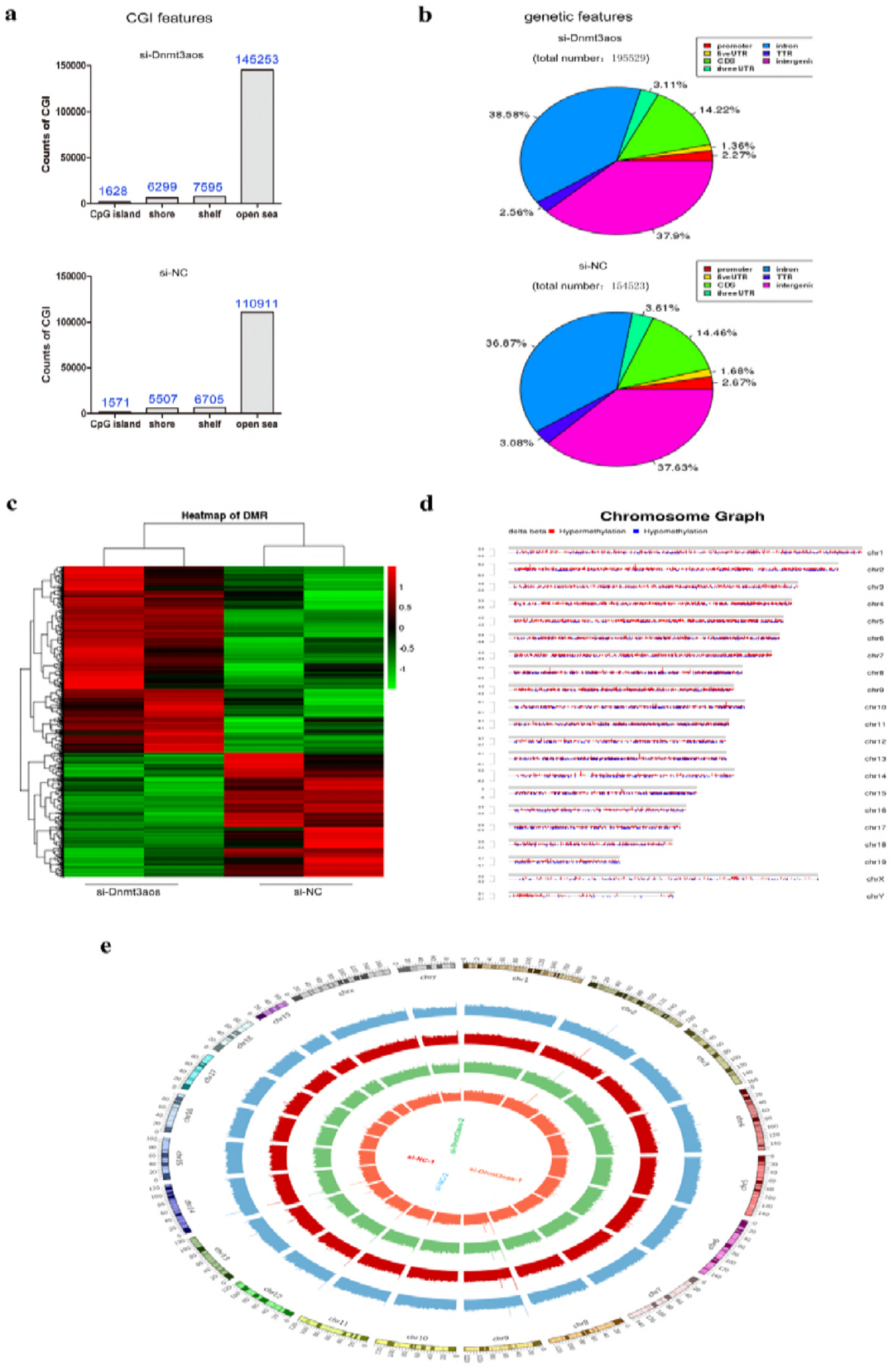

1027

1028

Fig 6.

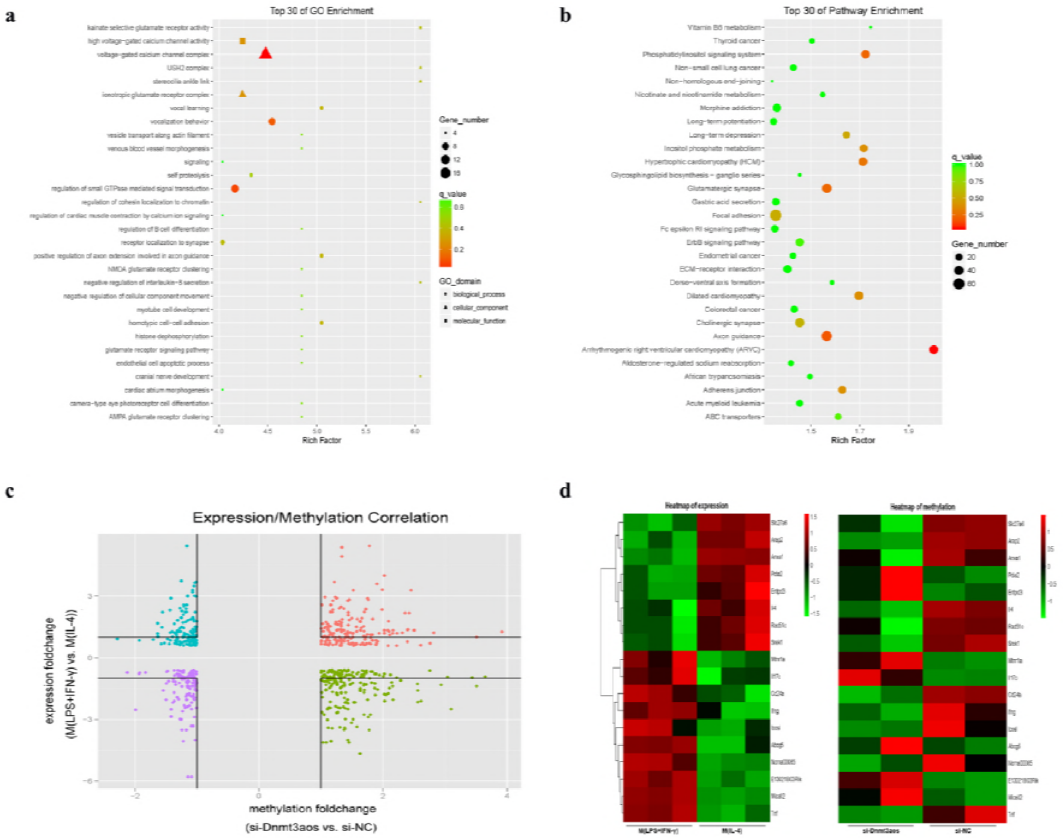

Fig 7.

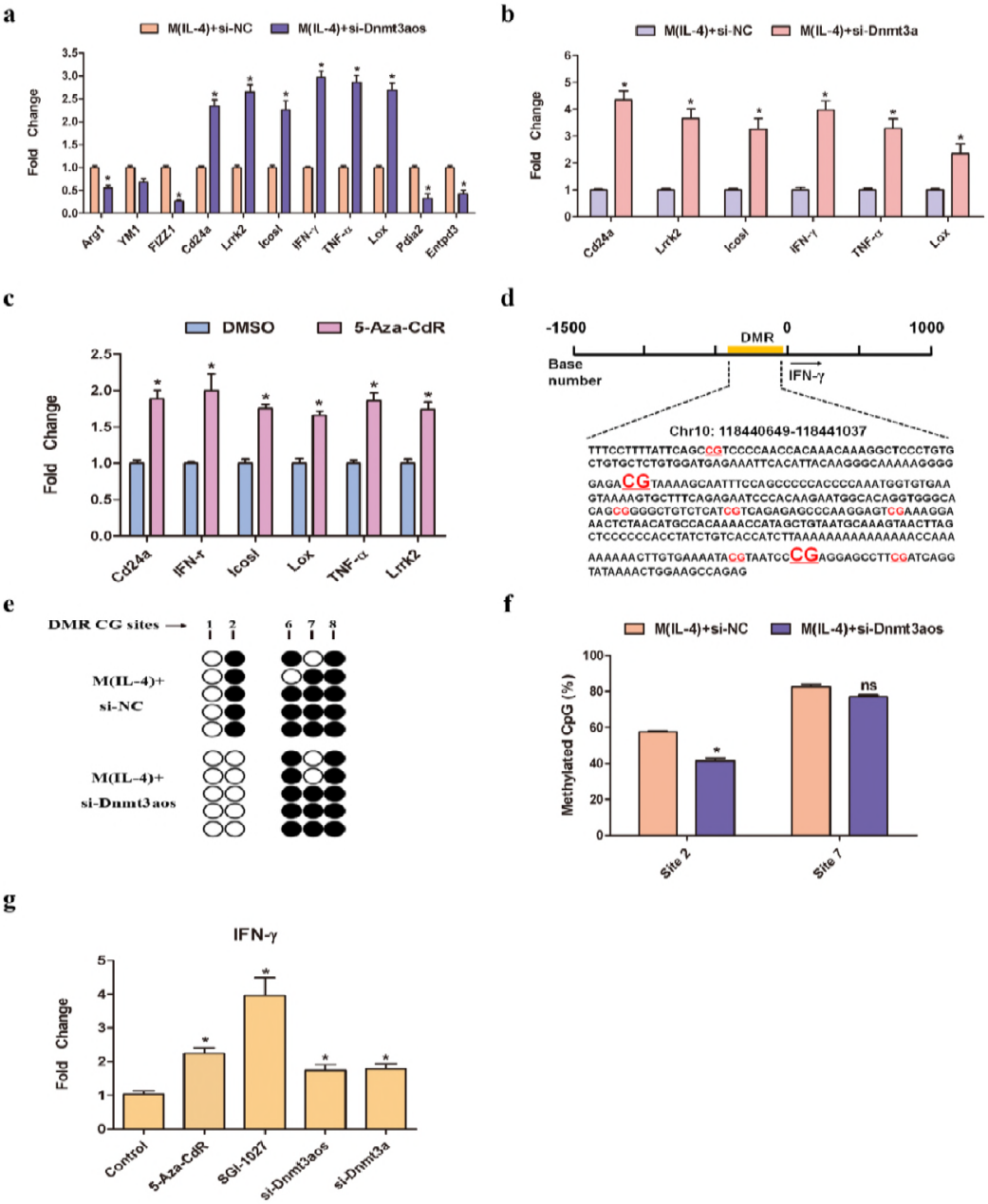

Supplementary Figure Legends

S1 Fig *Dnmt3aos* expression was detected in mouse tissues including lung, brain, spleen, pancreas, liver, heart, kidney, and fat. Error bars depict mean ± SD.

S2 Fig Relative gene expression during macrophage M(LPS+IFN-γ)/ M(IL-4) polarization. (a) Gene expression of iNOS or Arg1 following re-polarization of M(LPS+IFN-γ) macrophages to M(IL-4) macrophages by LPS/IFN-γ. **(b)** Gene expression of iNOS or Arg1 following re-polarization of M (IL-4) macrophages to M(LPS+IFN-γ) macrophages by LPS/IFN-γ. Data are representative of three separate experiments, and show the means ± SD, *P < 0.05, **P < 0.01, ***P < 0.001.

S3 Fig Identification of ex vivo-programmed M(LPS+IFN-γ) and M(IL-4) macrophages. BMDMs were cultured in the presence of LPS (100 ng/ml) plus IFN-γ (20 ng/m) or IL-4 (20 ng/ml). Polarization specific biomarkers were analyzed by RT-qPCR assays using RNA collected from BMDMs over different time courses post treatment. **(a)** iNOS **(b)** Arg1. Data are representative of three separate experiments and are compared to the control group.

S4 Fig *Dnmt3a* siRNA inhibition efficiency in BMDMs was examined by western blotting.

S5 Fig *Lox* and *Icosl* methylation profiles in the si-NC or si-Dnmt3aos transfected M(IL-4) macrophages. (a) The location and exhibition of DNA sequences of DMRs in the region of *Lox* obtained from MeDIP-seq enrichment. The CG sites (sites 1-2 in order) with underlining and red color were successfully BSP sequenced. **(b)** The open and filled circles symbolize the unmethylated and

1071 methylated CGs, respectively. Five colonies of separate CG sites from each group of
1072 *Lox* gene were further analyzed by BSP sequencing. **(c)** The location and exhibition of
1073 DNA sequences of DMRs in the region of *Icosl* obtained from MeDIP-seq enrichment.
1074 The CG sites (sites 1-24 in order) with underlining and red color were successfully
1075 BSP sequenced. **(d)** The open and filled circles symbolize the unmethylated and
1076 methylated CGs, respectively. Five colonies of separate CG sites from each group of
1077 *Icosl* gene were further analyzed by BSP sequencing.

1078 **S6 Fig *Cd24a* methylation profiles in the si-NC or si-Dnmt3aos transfected**
1079 **M(IL-4) macrophages. (a)** The location and exhibition of DNA sequences of DMRs
1080 in the promoter region of *Cd24a* obtained from MeDIP-seq enrichment. The CG sites
1081 (sites 1-12 in order) with underlining and red color were successfully BSP sequenced.
1082 **(b)** The open and filled circles symbolize the unmethylated and methylated CGs,
1083 respectively. Five colonies of separate CG sites from each group were further
1084 analyzed by BSP sequencing. **(c)** Pyrosequencing analysis of CG methylation level in
1085 the selected CG site of the *Cd24a* gene promoter from the BSP sequencing results.
1086 The figure illustrates the variation in methylation level at CG site 12 in si-NC or
1087 si-Dnmt3aos-transfected M(IL-4) macrophages.

1088 **S7 Fig *TNF-α* methylation profiles in si-NC or si-Dnmt3aos-transfected M(IL-4)**
1089 **macrophages. (a)** The location and exhibition of DNA sequences of DMRs in the
1090 promoter region of *TNF-α* obtained from MeDIP-seq enrichment. The CG sites (sites
1091 1-6 in order) with underlining and red color were successfully BSP sequenced. **(b)**
1092 The open and filled circles symbolize the unmethylated and methylated CGs

respectively. Five colonies of separate CG sites from each group were further analyzed by BSP sequencing. **(c)** Pyrosequencing analysis of CG methylation level in the selected CG site of the *TNF-α* gene promoter from the BSP sequencing results. The figure illustrates the variation in methylation levels at CG site 4 in si-NC or si-Dnmt3aos-transfected M(IL-4) macrophages.

S8 Fig *Lrrk2* methylation profiles in si-NC or si-Dnmt3aos-transfected M(IL-4) macrophages. (a) The location and exhibition of DNA sequences of DMRs of *Lrrk2* obtained from MeDIP-seq enrichment. The CG sites (sites 1-3 in order) with underlining and red color were successfully BSP sequenced. **(b)** The open and filled circles symbolize the unmethylated and methylated CGs, respectively. Five colonies of separate CG sites from each group were further analyzed by BSP sequencing. **(c)** Pyrosequencing analysis of CG methylation levels in the selected CG site of the *Lrrk2* gene from the BSP sequencing results. The figure illustrates the variation in methylation levels at CG site 3 in si-NC or si-Dnmt3aos-transfected M(IL-4) macrophages.

S1 Fig.

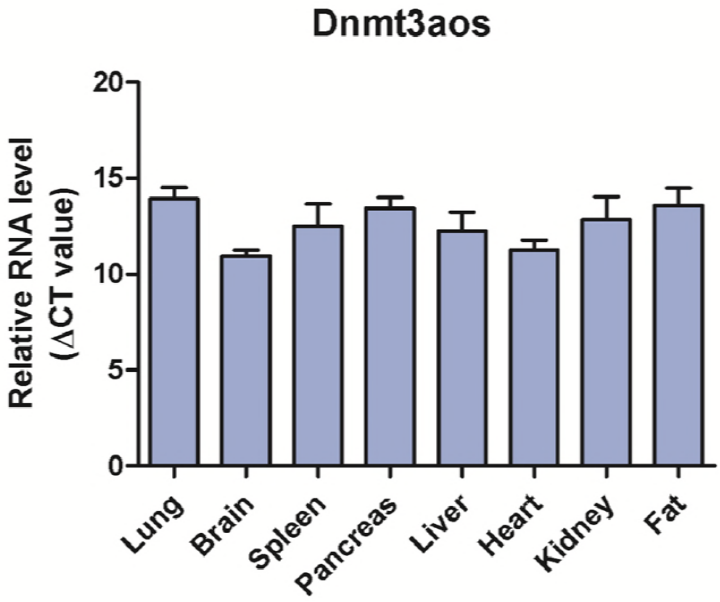

S2 Fig.

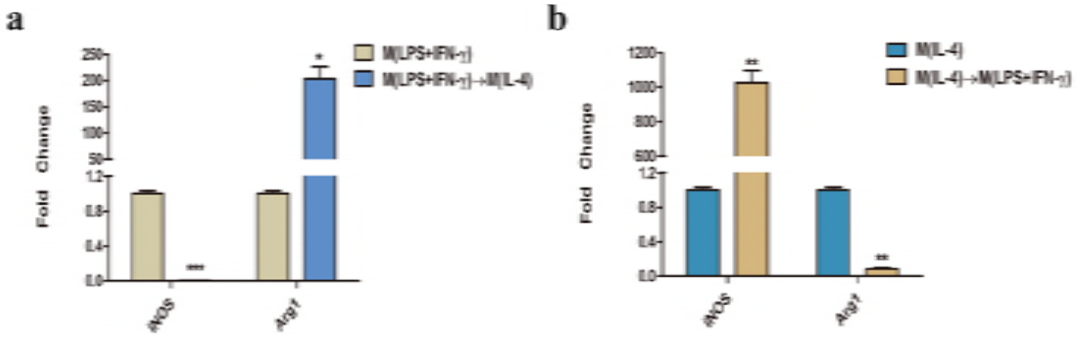

S3 Fig.

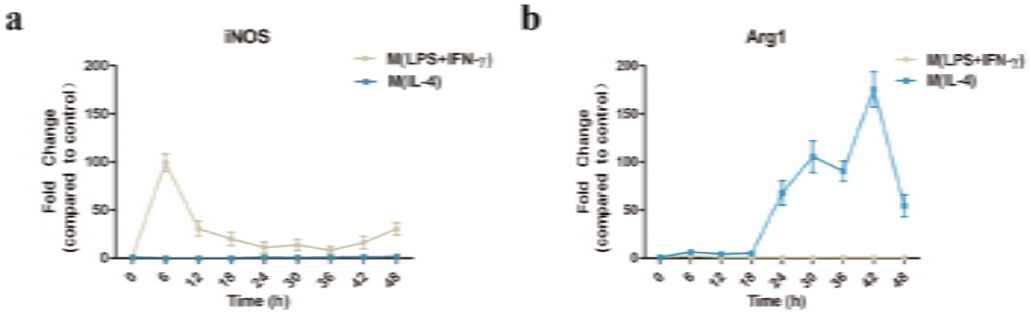

S4 Fig.

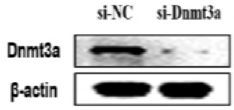

S5 Fig.

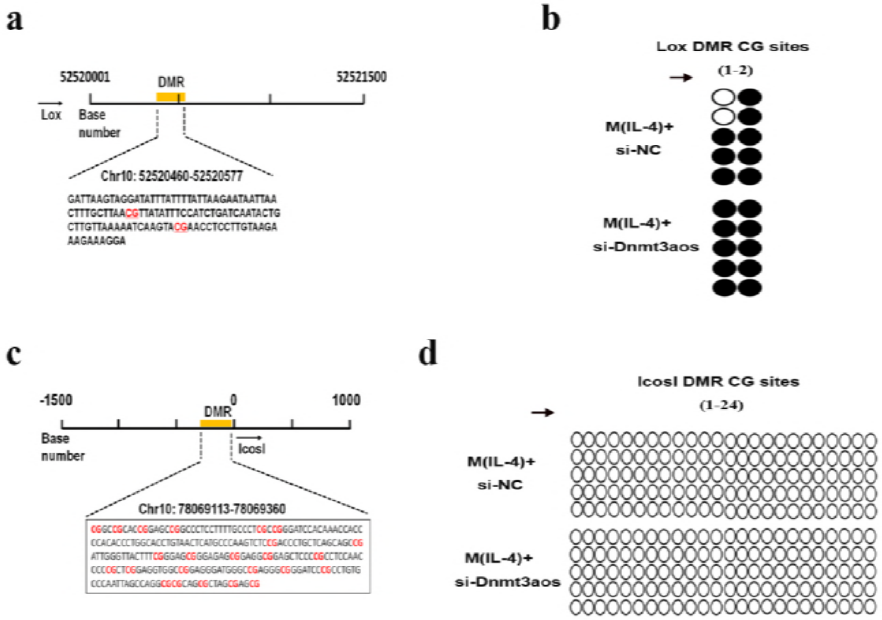

S6 Fig.

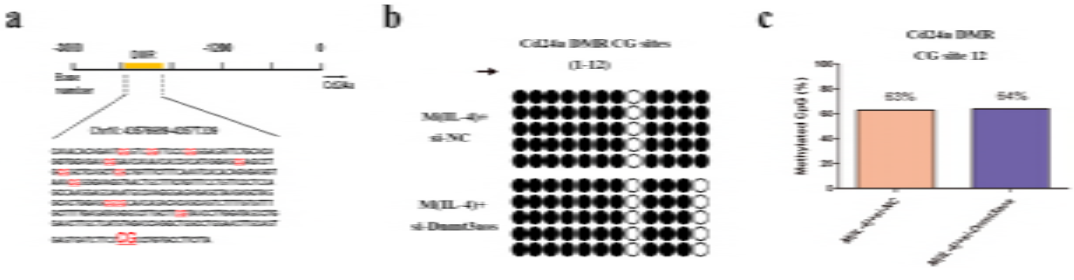

1133 **S7 Fig.**

1134 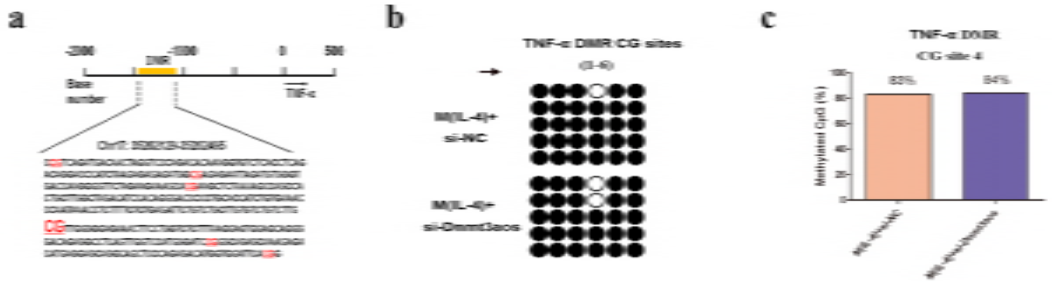

1135

1136 **S8 Fig.**

1137 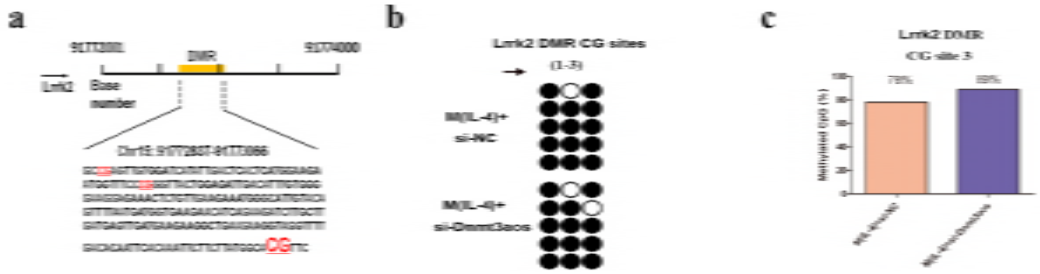

1138

1139

1140

1141

1142

1143

1144

1145

1146

1147

1148

Supplementary Tables

Supplementary Table S1. Primer sequences used in real-time PCR are written in 5'- 3' direction.

Genes	Primer (5'- 3')
AK048798	GACGGATGAGGAATGGGTTC
	TCCTGTGAAGTGTGGACTCT
AW112010	TCTTCTGCCATCAAGCCAAT
	TCTCTCCTGAACGACCCAGT
4933417E11Rik	CCAGAAGACACCGAAAGGAA
	GGATGTGCTGAGTGGAGTGA
Dnmt3aos	TCTCTAGACACCTCTCCCCT
	ACATGACACGTGACACCAAA
iNOS	ATCTTTGCCACCAAGATGGCCTGG
	TTCCTGTGCTGTGCTACAGTTCCG
TNF-α	CCAGTGTGGGAAGCTGTCTT
	AAGCAAAAGAGGAGGCAACA
IL-12	GATGTCACCTGCCCAACTG
	TGGTTTGATGATGTCCCTGA
Arg1	TGACTGAAGTAGACAAGCTGGGGAT
	CGACATCAAAGCTCAGGTGAATCGG
YM1	ATGAAGCATTGAATGGTCTGAAAG
	TGAATATCTGACGGTTCTGAGGAG
FIZZ1	AGGTCAAGGAACTTCTTGCCAATCC
	AAGCACACCCAGTAGCAGTCATCCC
Dnmt3a	GAGCAGTCTCAACAGCACCA
	CTGTGTGGTAGGCACCTGAA
GAPDH	GGTTGTCTCCTGCGACTTCA
	TGGTCCAGGGTTTCTTACTCC
U6	ATTGGAACGATACAGAGAAGATT
	GGAACGCTTCACGAATTTG
IFN-γ	GTTACTGCCACGGCACAGTCATTG
	ACCATCCTTTTGCCAGTTCCTCCAG
Cd24a	CATCTGTTGCACCGTTTCC
	GAGAGAGAGCCAGGAGACCA
Icosl	CACCTGTCATCAGCACCTCT
	GGCTATTGTCCGTTGTGTTG
Lrrk2	CCAGACCAACCAAGGCTCACTATTC
	ACAGCCACTTCCTCTCCTTCGTAG
Lox	CAGAGGAGAGTGGCTGAAGG
	CTGCCGCATAGGTGTCATAA

Pdia2	CCAGTCAAGACTCTCGTGAGCAAG GCATCCAACTCGGCAATGACAATG
Entpd3	CCAAGAGCAAGACGCCTGTTCC CTGTGTAGTAGAAGCCTGCGAACG

Supplementary Table S2. **Oligonucleotides sequences used in siRNA transfection are written.**

Genes	Target sequences
Dnmt3aos smart silencer	GGACTCACTTCCTGTTGGT CACCAACATGCATCACTTT GCTGTTACATGCTCTAACA TCATGGGTGGTTCCTGCCAG TGACCAACTTGGGAGGCACT TGTGCTGGCAACTAGTGGAT
Dnmt3a	CATCCACTGTGAATGATAA

Supplementary Table S3. **Primer sequences used in BSP sequencing are written.**

Genes	Primer
IFN-γ	CCTCATGGTTTGAGAAGCCCAAGAG GATCAGGTATAAAACTGGAAGCCAGAG
Cd24a	TGGGCACAGAATGGCCAACATCCTG GAGCTTGGTTTCCAGGCATGCACTATC
TNF-α	TAGAAAGAGGGGAAAAATAGAAAG GAGTGAGGCAGCTTAACTGCCGGAG
Lrrk2	TCTAATGTAGGTTGTATTCTTCTGG GCTATATTTACATGACTTTAATATATAAGAGTCATT

Supplementary Table S4. **Primer sequences used in Pyrosequencing are written.**

Genes	Primer
IFN-γ (CG site2)	AYGTAAAAGTAA
IFN-γ (CG site7)	TTYGAGGAG

Cd24a (CG site12)	TYGTTTGTG
TNF-α (CG site4)	TAYGTTCG
Lrrk2 (CG site3)	YGTTGGGGGA

1159